CHALMERS
UNIVERSITY OF TECHNOLOGY

Parameter estimation using a self-commissioning sequence for internal permanent magnet synchronous motors

Determining the inductances L_d, L_q and the stator resistance R_S required to tune a PI current regulator, using high frequency voltage source inverter noise

Master's thesis in Systems, Control & Mechatronics

ALEX ERIXON, ALFRED LIND-ANDERTON

Department of Electrical Engineering

CHALMERS UNIVERSITY OF TECHNOLOGY
Gothenburg, Sweden 2022
www.chalmers.se

Master's thesis 2022

Parameter estimation using a self-commissioning sequence for internal permanent magnet synchronous motors

Determining the inductances L_d, L_q and the stator resistance R_S required to tune a PI current regulator, using high frequency voltage source inverter noise

ALEX ERIXON, ALFRED LIND-ANDERTON

CHALMERS
UNIVERSITY OF TECHNOLOGY

Department of Electrical Engineering
Division of Systems and Control
Chalmers University of Technology
Gothenburg, Sweden 2022

Parameter estimation using a self-commissioning sequence for internal permanent magnet synchronous motors
Determining the inductances L_d, L_q and the stator resistance R_S required to tune a PI current regulator, using high frequency voltage source inverter noise
ALEX ERIXON
ALFRED LIND-ANDERTON

Supervisor: Daniel Chädström, Aros Electronics AB
Examiner: Torbjörn Thiringer, Department of Electrical Engineering

Master's Thesis 2022
Department of Electrical engineering
Division of Systems and Systems and Control
Chalmers University of Technology
SE-412 96 Gothenburg
Telephone +46 31 772 1000

Typeset in LaTeX
Printed by Chalmers Reproservice
Gothenburg, Sweden 2022

Parameter estimation using a selfcommissioning sequence for internal permanent magnet synchronous motors
Determining the inductances L_d, L_q and the stator resistance R_S required to tune a PI current regulator, using high frequency voltage source inverter noise

ALEX ERIXON
ALFRED LIND-ANDERTON
Department of Electrical Engineering
Chalmers University of Technology

Abstract

In this thesis, a self-commissioning method for an electrical permanent magnet synchronous motor (PMSM) is tested and verified. The self-commissioning method estimates the stator resistance R_s and inductances L_d and L_q to allow a PI current controller to be implemented. The methodology proposed is inspired by the method of Voltage Source Inverter (VSI)-driven Standstill Frequency Response (SFR) offline estimation and it performed without any extra equipment at standstill. First, initial rough estimates of the parameters are calculated based on the rated data or alternatively, voltage probing is used to get the parameters. This allows for a current PI-regulator to be automatically designed. With a working current controller the motor can be held still using a locking current in the d-axis, which ensures a stationary rotor. For the inductances, a high frequency noise is applied in both the d- and q-direction to excite the motor with current, without making the rotor move. The current responses recorded from this noise and the response from simply varying the locking current without any noise, is filtered using least squares (LS) method and allows for the inductances and resistance to be calculated.

The results show that the inductances and the stator resistance can be estimated using the proposed method, with the estimates being accurate enough to design a well behaving PI current regulator. However, the initial rough parameters cannot be estimated using the proposed calculation method and requires the voltage probing to accurately execute the methodology using the current regulator. It is possible to tune the PI regulator using the voltage probing method, but the accuracy is lower. Finally, it can be shown that rotating the rotor to align the theoretical inductance positions with a phase of the motor increases the accuracy of the inductance. Therefore, the highest accuracy is achived by completing the full method proposed using the initial voltage probing whereafter the locking current is manipulated such that both noises align with a single phase.

Keywords: permanent magnet synchronous motor (PMSM), auto-tuning, parameter estimation, sensorless control, initial rotor position detection, self-commissioning sequence, current regulator, PID

Acknowledgements

This work has been conducted at Aros Electronics AB and the Department of Energy and Environment at Chalmers University of Technology. We are grateful for the assistance and the introduction into the field that Daniel Chädström, Filip Karlsson and Mikael Alatalo at Aros that they provided. Finally, we would like to thank Torbjörn Thiringer at the Department of Electrical Engineering for his guidance throughout this project.

Alex Erixon & Alfred Lind-Anderton, Gothenburg, June 2022

List of Acronyms

Below is the list of acronyms that have been used throughout this thesis listed in alphabetical order:

PMSM	Permanent Magnet Synchronous Motors
SFR	Standstill Frequency-Response
VSI	Voltage Source Inverter
FEM	Finite Element Method
RMS	Root Mean Square
MOSFET	Metal-Oxide Semiconductor Field-Effect Transistor
IGBT	Insulated-gate Bipolar Transistor
PWM	Pulse Width Modulation
PID	Proportional Integral Derivative
LS	Least Squares
SRAM	Static Random-Access Memory
LCR	Inductance Capacitance Resistance

Contents

1
Introduction

1.1 Problem background

Permanent magnet synchronous motors (PMSMs) are attractive for industrial application due to their simplicity, high efficiency, and high power factor. They do however require both the position and speed of the rotor to be controlled effectively [1] [2]. These states can be measured using sensors such as encoders or Hall effect sensors, but leads to increased costs, complexity and decreased robustness of the system by their susceptibility to fail due to temperature, vibration and similar effects from their environment [2].

The company Aros Electronics AB develops software for sensorless control of PMSMs as part of the power solutions they provide. Since no position sensor is mounted on the shaft, the rotor position is unknown. The rotor position is the direction of the magnetic flux from the rotor magnets relative to the stator winding coils.

The PI current controllers used in such applications to need to have their K_P and K_I parameters properly designed, and for that the plant parameters must be known. Thus the inductances in the d- and q-direction in the dq-system L_d and L_q together with the stator winding resistance R_s need to be known in advance or estimated by some software algorithm. The same data is necessary for the rotor speed and position estimators. However, several circumstances limit the availability of all of the PMSM's precise nominal parameters. In this aspect, manufacturing tolerances and variations cause differences in motor parameters even among PMSMs from the same production batch [3]. Furthermore, the producers of commercially manufactured machines provide very little information to motor-drive designers that want to attain a high level of control efficiency [4]. The rated output power, speed, maximum speed, input voltage, current, protection level, dimension, and weight are often provided by the manufacturer.

Despite the fact that the nominal PMSM parameters are accessible for control design, the parameters fluctuate nonlinearly based on the operating environment (e.g. temperature) and operating conditions (e.g., speed and load torque) [5] [6]. High temperatures, for example, might raise the value of the stator resistance while also lowering the rotor flux linkage by demagnetizing the permanent magnet (PM) and dq-axis inductances, potentially causing torque ripples [7] [8]. Hence Aros desire to quickly and effectively deploy a new PMSM or use an existing one with a different load, where they seek to find a way to automate the measuring and/or estimation

of the aforementioned parameters. To allow for this fast application, they desire that the method requires no additional or task-specific equipment and only use the hardware available on the controlboard for the motor.

1.2 Previous work

Aros today uses a manual method to calculate the motor parameters with the help of general measurement equipment. The method is time-consuming, and requires physical user manipulation of the rotor which might be inaccurate and inconsistent.

Parameter estimation is often categorized into offline estimation and online estimation and the different subvariants will be further discussed. Offline estimation is usually done by removing the PMSM from its load application and/or at standstill. Frequency domain-based, time domain-based, and finite-element methods are the three types of offline parameter identification methods [9]. Standstill frequency-response (SFR) is the dominant method when it comes to frequency domain-based methods. Where methods can further be divided into power-amplifier-driver SFR and voltage source inverter (VSI) SFR, with instructions available to perform the SFR tests according to the IEEE Standard [10]. SFR is performed by evaluating the response of a test signal with a single frequency from a predetermined set of signal frequencies in a sequential manner [11]. By sampling the excitation pulse responses the parameters can be derived. Although SFR tests necessitates a high number of measurements and long measurement times it provides a well-performing result. Some kind of regression like Maximum Likelihood (ML) or Least Squares (LS) method is often performed with the measured data to filter out unwanted data and to make it more reliable [12]. The power-amplifier-driven SFR [13] and the VSI-driven SFR [10] are widely utilized in the industry for self-commissioning and condition monitoring of PMSM drives.

Regarding time domain-based methods, the most common methods are the search coil test [14], load test [15], phase voltage measurement test [16], AC standstill test [17], locked-rotor test [17], DC-biased AC signal injection test [18] and torque test[19]. All these tests besides the phase voltage measurement test require extra equipment or the PMSM is configured to run at a constant speed to be performed. Either the rotor must be locking with a counter working motor or different sensors such as torque sensor need to be added, or varying loads have to be attached [20][21].

With the knowledge of the structure, geometry and design of the PMSMs the finite element method (FEM) can determine and analyze the parameters [22]. By exciting the magnets in the motor with currents, magnetic fields are created and studied, this combined with the knowledge of the mechanical properties of the PMSM allows for the parameters to be extracted. Due to the effects of magnetic saturation, mutual inductances and the change in magnetic flux needs to be considered and acted on accordingly [23]. Popular FEM methods are the stored magnetic energy method [24], energy perturbation method [25], and airgap flux density method [22].

The methods that derive the parameters during operation are called online estimation methods. The online technique is used to find the precise, updated parameters for the robust control design since the model parameters in the PMSMs change due to temperature and nonlinearities. There are several proposed methods of this nature, and the most common ones are spectral analysis, observer-based system, and model reference adaptive system (MRAS). The adaptation mechanism in MRAS is usually linear, with neural networks (NN) proved to be effective for parameter identification in nonlinear systems. In the work by Elbuluk et. al. [26] there is a proposed MRAS algorithm with NN as the adaptive mechanism. A NN-based method is proposed in [27]. [28] proposes particle swarm optimization-based parameter identification for PMSM, while [29] presents a fuzzy hybrid swarm optimization technique. The observer-based system uses the well known Extended Kalman Filter (EKF) and is especially good in noisy environments [30].

1.3 Aim and Scope

The aim of the thesis is to find a suitable self-commissioning method to implement in Aros' existing control software. The goal is that the self-commissioning procedure can estimate the previously mentioned motor parameters, for an arbitrarily chosen PMSM. This should be achieved without any extra equipment apart from the control board with inverter used in operation, accurately enough that a well behaved PI-regulator can be tuned. The method/-s will be tested and verified on a psychical motor, as well as in a simulation environment. Data from other motors will be used as a comparison study for some parts of the method.

1.4 Limitations

This thesis work is subject to the following limitations:

- The motor available for verifying the self commissioning algorithm is limited to the one motor Aros can provide.
- The current motor control algorithm developed and used by Aros must be used to be able to drive the proprietary control board.

2
Theory

2.1 Permanent Magnet Synchronous Motor

This chapter will explain briefly how PMSMs can be controlled by three-phase motor control.

2.1.1 Space vectors and three-phase system

The PMSM is a three-phase electric motor. For each of the phase, the basic principle is to use sinusoidal AC currents separated by 120° . Electric motor windings are insulated wires wrapped around a magnetic core. These cables provide a path for electric current to flow while also creating a magnetic field that spins the rotor of the motor. Each winding can be represented as a series of inductance with a resistance [31], and is visualized in Fig. 2.1.

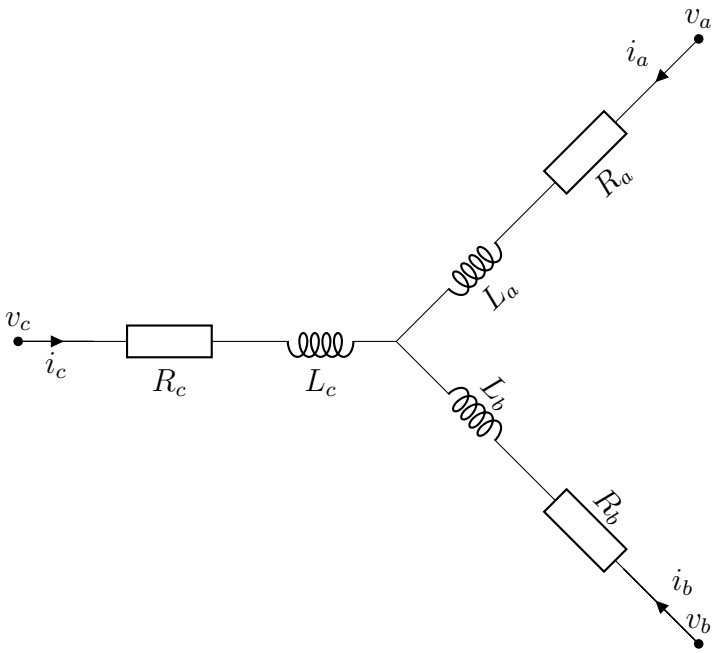

Figure 2.1: Winding of a three-phase system with the resistances R_x and inductances L_x for the three phases A,B,C

Faraday's law [31] states that when a current passes through a coil, it produces a magnetic field. The permanent magnets used in the PMSM have their own magnetic

fields, and if the fields' opposite poles are not perfectly aligned, the interaction of these fields produces a torque. Simply put, when the magnetic field formed by a coil is 90° ahead of the permanent magnet's north pole orientation, this effect is strongest thus produces the most torque [31]. To maintain the rotation of the rotor, the two magnetic fields should reject each other at all times. One of the reasons for using the three-phase system is that the instantaneous three-phase power is constant, making the motor move smoothly regardless of rotor position. The relationship between power and torque is proportional, making it an efficient way to drive an motor. Additionally, using Kirchhoff's current equation and Fig 2.1, it is easy to demonstrate that the currents are linearly dependent according to

$$i_a + i_b + i_c = 0. \tag{2.1}$$

As a result, the three-phase motor can be represented using a two-phase system with perpendicular axes, since the vectors can be expressed using the other two, e.g. $i_a = i_b + i_c$.These are denoted α and β. By considering these as the real and imaginary axes in a complex plane for modeling purposes and the current vector becomes $i^s = i_\alpha + ji_\beta$, also known as the space vector. The stator fixed coordinates are indicated by the superscript s and can be written as a real-valued vector $i^s = \begin{bmatrix} i_\alpha & i_\beta \end{bmatrix}^T$. Since imaginary numbers are avoided in this form, it is more suited for controller implementation. Using phasor arithmetic, the transformation between the three-phase system and the $\alpha\beta$-system is obtained by

$$i_\alpha + ji_\beta = \frac{2}{3}K\left[i_a + e^{j2\pi/3}i_b + e^{j4\pi/3}i_c\right], \tag{2.2}$$

where K is a selected scaling constant [31]. Depending on the application, it is utilized to make two-phase system calculations easier. Peak-value scaling ($K = 1$), RMS-value scaling ($K = \frac{1}{\sqrt{2}}$), and Power-invariant scaling ($K = \sqrt{3/2}$) are the three most prevalent options [31]. A constant transformation matrix is used to transform the real-valued space vector

$$\begin{bmatrix} i_\alpha \\ i_\beta \end{bmatrix} = K \begin{bmatrix} \frac{2}{3} & -\frac{1}{3} & -\frac{1}{3} \\ 0 & \frac{1}{\sqrt{3}} & -\frac{1}{\sqrt{3}} \end{bmatrix} \begin{bmatrix} i_a \\ i_b \\ i_c \end{bmatrix}. \tag{2.3}$$

2.1.2 DQ coordinate system

The current vector in the phasor diagram should rotate at the same speed as the rotor and have a phase lead of around 90 degrees when compared to the rotor heading to sustain a constant speed [31]. It would be advantageous to employ rotor-fixed coordinates for control reasons since such a coordinate system would rotate at the same speed as the rotor. The currents are then at constant speed rather than oscillating as they are in the $\alpha\beta$-system, resulting in a simplified representation of the system. By defining the current vector that has been rotated

$$\mathbf{i} = e^{-j\theta_r}\mathbf{i}^s \triangleq i_d + ji_q \tag{2.4}$$

this can be achieved [31]. The dq coordinate system is defined as follows: i_d is the current in the rotor heading direction, and i_q is the current in the perpendicular direction, which is always 90 degrees ahead of the north pole of the magnet. As a result, i_q is the torque-producing current. The relationship between the stator fixed coordinate system and the rotor fixed dq coordinate system is shown in Fig. 2.2. The electrical angle, θ_r in Fig. 2.2, is proportional to the rotor angle, θ_m, and the number of pole pairs, n_p. The rotor angle is the angle formed by the rotor heading and the fixed $\alpha-$axis of the stator. The rotor angle, θ_r, must be known to make the transition from the $\alpha\beta$-system to the dq-system. The transformation between both systems is a simple rotation, as in Fig. 2.2, or the rotational matrix for the real-valued vector representation

$$\begin{bmatrix} i_d \\ i_q \end{bmatrix} = \begin{bmatrix} \cos(\theta_r) & \sin(\theta_r) \\ -\sin(\theta_r) & \cos(\theta_r) \end{bmatrix} \begin{bmatrix} i_\alpha \\ i_\beta \end{bmatrix}. \tag{2.5}$$

The rotor-fixed dq-frame will be used throughout the rest of this report since it is more convenient for control and simplifies computations.

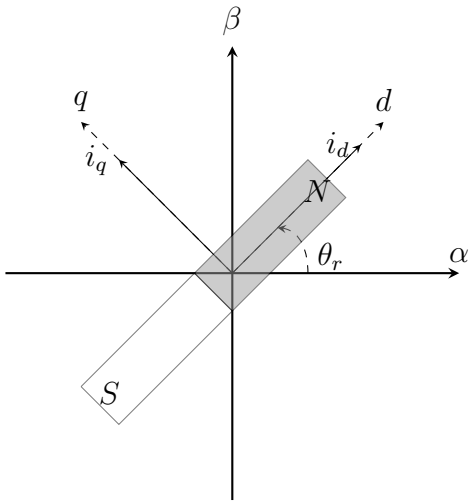

Figure 2.2: Rotor magnet excited and aligned with the d-direction in a $\alpha\beta$-system

2.1.3 Dynamic Model for the PMSM

The voltage across the stator windings is the PMSM's input signal. According to the law of induction, a voltage that does not dissipate in the winding resistance produces magnetic flux. As a result, the voltage equation can be expressed as [31]

$$\mathbf{v}_s^s - R_s \mathbf{i}_s^s - \frac{d\boldsymbol{\psi}_s^s}{dt} = 0, \tag{2.6}$$

where s denotes the vectors expressed in the stator bound coordinate system. The stator flux $\boldsymbol{\psi}_s^s$ is given by

$$\boldsymbol{\psi}_s^s = L_s \mathbf{i}_s^s + \boldsymbol{\psi}_R^s \tag{2.7}$$

with the stator inductance denoted as L_s and the rotor flux linkage $\boldsymbol{\psi}_R^s$ being produced by permanent magnets. As shown in Fig.2.2, the rotor flux determines the d axis, which is displaced by the flux angle θ relative to the α-axis. As a result, $\psi_R^s = \psi e^{j\theta}$ is the rotor flux vector. For a constant L_s, the flux modulus ψ_R can be considered to be constant,

$$\frac{d\boldsymbol{\psi}_s^s}{dt} = L_s \frac{d\mathbf{i}_s^s}{dt} + j\omega_r \psi_R e^{j\theta} \tag{2.8}$$

where $\omega = \dot{\theta}$. Equation (2.6) can then be written as

$$L_s \frac{d\mathbf{i}_s^s}{dt} = \mathbf{v}_s^s - R_s \mathbf{i}_s^s - \underbrace{j\omega_r \psi_R e^{j\theta}}_{\mathbf{E}^s} \tag{2.9}$$

where $\mathbf{E}^s = j\omega_r \psi_R e^{j\theta}$ is the back electromotive force (emf) or the current produced in the opposite direction by the rotation of the rotor. The dynamic equivalent circuit that is shown in Fig. 2.3 can be used to represent this relationship.

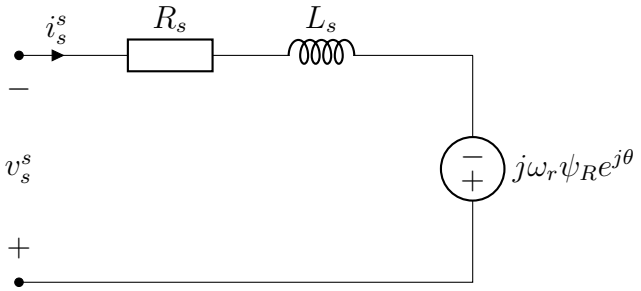

Figure 2.3: Dynamic equivalent circuit for the round-rotor PMSM

When developing a controller for the PMSM, it is convenient to employ synchronous, i.e. rotor fixed, coordinates, as discussed in Chapter 2.1.2. By rotating all stator coordinates with the angle θ, the electrical dynamics in equation (2.9) are translated into dq-coordinates, yielding

$$L_s \frac{d\left(e^{j\theta_r}\mathbf{i}\right)}{dt} = jL_s\omega_r e^{j\theta_r}\mathbf{i} + L_s e^{j\theta_r}\frac{d\mathbf{i}}{dt} = e^{j\theta_r}\mathbf{v} - R_s e^{j\theta_r}\mathbf{i} - j\omega_r\psi_R e^{j\theta_r} \tag{2.10}$$

and is multiplied by $e^{-j\theta_r}$ to make it more convenient and resulting in

$$L_s \frac{d\mathbf{i}}{dt} = \mathbf{v} - R_s\mathbf{i} - jL_s\omega_r\mathbf{i} - j\omega_r\psi_R. \tag{2.11}$$

This is written as $\mathbf{i} = (i_d + ji_q)$ in a complex equation. That is, imaginary numbers indicate the current's q-direction, while real numbers reflect the current's d-direction. A real-valued vector representation is preferable for control implementation, as indicated in Chapter 2.1.2, and (2.10) can instead be represented as

$$L_s \frac{d}{dt}\begin{bmatrix} i_d \\ i_q \end{bmatrix} = \begin{bmatrix} v_d \\ v_q \end{bmatrix} - R_s \begin{bmatrix} i_d \\ i_q \end{bmatrix} - L_s\omega_r \begin{bmatrix} -i_q \\ i_d \end{bmatrix} - \begin{bmatrix} 0 \\ \psi_R\omega_r \end{bmatrix}. \tag{2.12}$$

Both directions of resistance can be modeled as equal, making it possible to simplify the calculations and use the same R_s in both d and q directions. The stator inductance, however, cannot be modeled as equal in both directions. That is because the magnets in the rotor aren't evenly distributed throughout the entire surface and the inductance varies sinusoidally depending on the rotor angle θ_r. The inductance on the d and q axis is denoted by L_d and L_q, respectively, and the subscript inductance L_s can be written as a matrix

$$L_s = \begin{bmatrix} L_d & 0 \\ 0 & L_q \end{bmatrix} \tag{2.13}$$

and in component form, it results in

$$L_d \frac{di_d}{dt} = u_d - R_s i_d + \omega_r L_q i_q \tag{2.14}$$

$$L_q \frac{di_q}{dt} = u_q - R_s i_q - \omega_r \left(L_d i_d + \psi_R \right). \tag{2.15}$$

With help of the equations (2.14) and (2.15), the inductance can be calculated, the value is later used for tuning the PI-regulator and will be further explained in Chapter 2.2. The equations can also be represented as equivalent circuits seen in Fig. 2.4. The d and q axes, however, require different circuits due to their saliency.

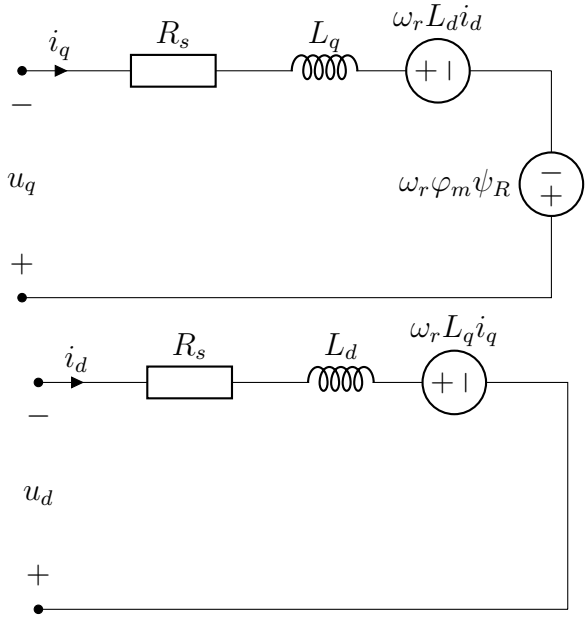

Figure 2.4: Dynamic equivalent circuits for the salient PMSM.

2.2 Current control

Since the desired AC currents for electrical equipment often vary from currents available from the grid in that region or other power sources such as generators or batteries, the power must be converted to the correct voltage, frequency, and phase.

An example of such an issue is providing the power to a variable-speed ac drive i.e. a PMSM, where the problem can be solved using an inverter. It utilizes switches and diodes to convert easily replicable DC-current to a range of different AC currents, varying in voltage, frequency, and phase [31]. Such an inverter can be seen in the left half of Fig. 2.5, consisting of three separate half-bridges connected together, as is the type used for a three-phase PMSM. Each half-bridge has a switch, where the choice between a MOSFET, IGBT, or other types of semiconductors is made based on the switching frequency, efficiency, or power throughput required for the application [32]. The switch is connected in parallel with a diode at both the upper and lower end of the line as can be seen in Fig. 2.5. By operating the semiconductors as switches, in a function similar to a relay, the current on the line can be controlled. If both the upper and lower switch on a line that leads to the A-winding, i.e. one phase of the motor, the line would short-circuit and no current would pass through the winding. Similarly, if only the upper switch on the A-line and the lower of the B-line were to be opened, the current would instead flow through the A-winding of the motor creating a positive current i_A while taking the reverse path through the B-winding creating a negative current i_B. The diodes prevent the current from flowing in the wrong direction by ensuring that the current will only flow through the turned-on switches. This allows for the manipulation of a DC-current to flow in both the positive and negative direction without interfering with the source [31].

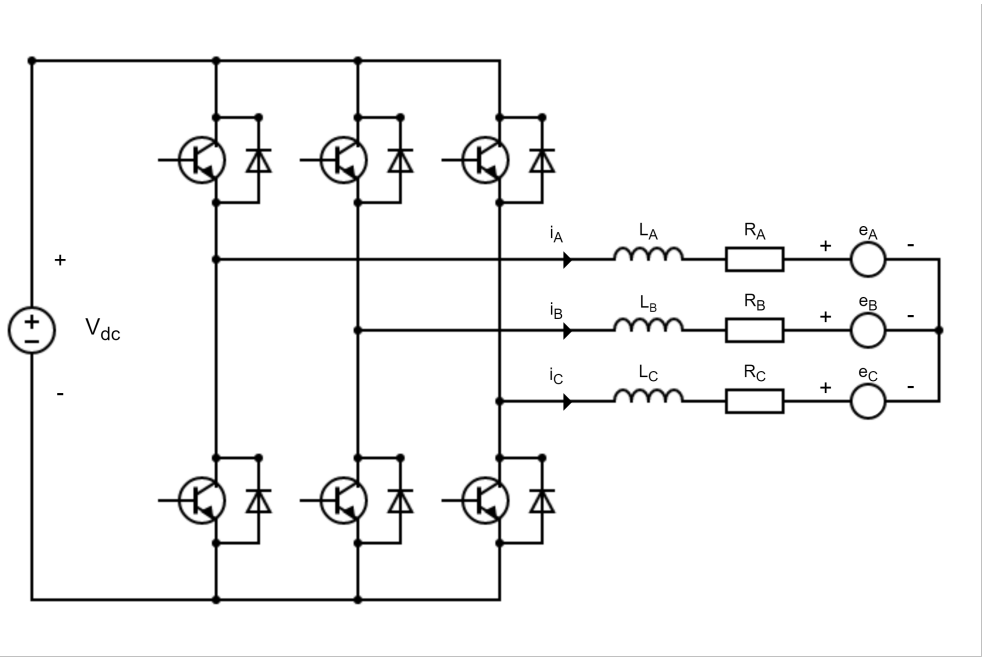

Figure 2.5: Schematic of a three-phase inverter connected to a three-phase PMSM

By controlling both the direction and the so-called duty cycle, a measurement of how long the switches are to be open for as part of a defined period expressed as a percentage, a practice called pulse width modulation (PWM). However, the time it takes for the different switches to change may vary which creates a small delay. This delay is called the dead-time and has an influence on the actual voltage applied, introducing an error compared to the desired voltage. A DC current can be

converted to sinusoidal AC-current by varying the duty cycle such that the voltage applied is equal to the mean voltage of the interval for the corresponding period. Similarly, the amplitude of the signal can be varied by varying the duty cycles. The mean values then become the desired wave as can be seen in Fig. 2.6. With a switching frequency being sufficiently high the result will be a smooth operation of the slower mechanics of the motor [31].

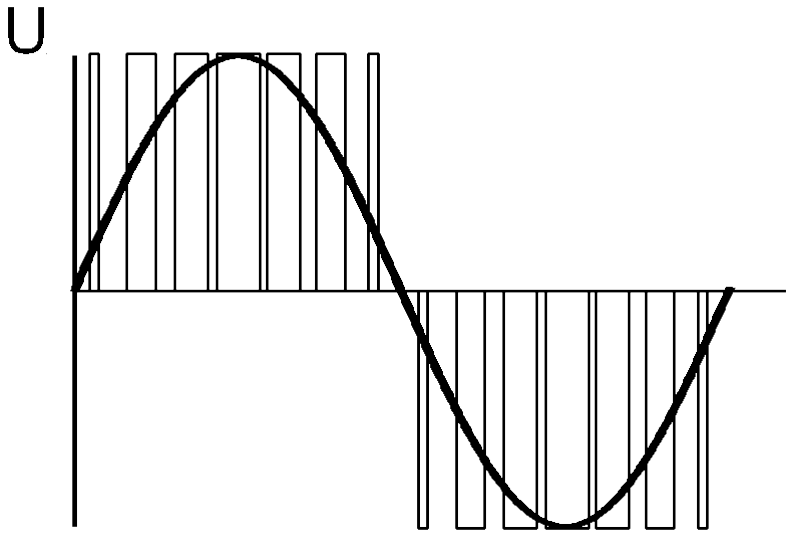

Figure 2.6: Sinusodial AC-current created using pulse width modulation.

Given an unknown resistance and inductance in the motor, the current response of an applied voltage cannot be calculated or estimated. This might result in high currents that could damage or destroy the components in the motor or the inverter rendering the test useless. The relation between the voltage and current in the d-axis in the synchronously rotating reference frame is

$$u_d = R_s i_d + \frac{d\varphi_d}{dt} - \omega_e \varphi_q \tag{2.16}$$

where R_s is the stator resistance which would be unknown, φ being the flux linkage in the d and q axes respectively in the previously mentioned reference frame, and ω_e being the electrical angular velocity. In the initial case, it is assumed that the motor is stationary since there is no way of controlling the motor without utilizing an external force, a method that would require added complexity and-/or setup to execute accurately. Additionally, the flux linkage in the d-axis is equal to the inductance times the current in the d-direction, therefore the above equation can be rewritten as

$$u_d = R_s i_d + L_d \frac{di_d}{dt} \tag{2.17}$$

showing that a current response will be proportional to the voltage with a factor equal to the resistance if the system is allowed to settle. Therefore an initial low voltage can be applied which would be carefully incremented allowing the current response to be measured, subsequently the relation between the current and voltage

for a mechanical and electrical stationary system can be determined. However, this approach cannot handle dynamic systems, which the majority of the motor's operational time is. A closed-loop system is beneficial and since the current is the determining output, a current controller similar to what is shown in Fig. 2.7.

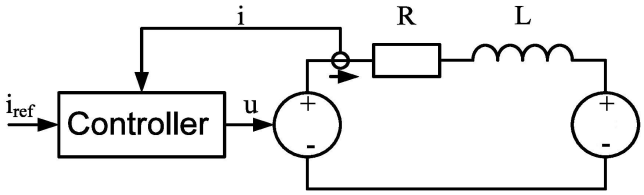

Figure 2.7: A current controller added to a RL-circuit with a load.

Since the computational power is limited in a system such as the one available for our application, the choice of the control algorithm is limited. Additionally the fairly simple system can be discretized into a single input single output (SISO) system, allowing for a variation of the widely used PID controller to be utilized. The controller uses the proportional (P), integrated (I) and derivative (D) of the error between the reference and true signal to create the control signal. The simplest version only uses the proportional gain. However, this approach often leaves residual error depending on the gain-value chosen and the operating point of the system. This can be resolved by adding an integrator gain, this gain as its name suggests depend on the error over time and will increase the control signal as long as there is a persisting error. The resulting PI controller is what is utilized by Aros to control their current, position, and speed, due to its simplicity and relatively good accuracy. Added to this control structure is a voltage limiter to prevent higher duty cycles than the inverter can handle.

2.3 Least squares

When trying to find a model to describe a system or simply a relationship between two or more things, a larger selection of data points reduces the influence of outliers or other types of errors [33]. However, with more data the problem of identifying characteristics or relations becomes greater if no specific methodology is introduced. For simpler systems where a curve-fitting would suffice i.e. the relationship between in and out data can be described by a polynomial, a maximum likelihood estimator (MLE) could be used. The estimator's approximates of the parameters become more accurate the larger the sample size is [34], however, the same can be achieved with the method of Least Squares (LS) [33]. The LS algorithm is one the most popular within the field of statistics [35] and will be implemented here mainly due to its simplicity and ease of implementation. Given a system of inputs X and related outputs Y the relationship between the predicted output $\hat{Y}$ and inputs can be described by

$$\hat{Y} = kX + m \tag{2.18}$$

where the slope k and interception m can be decided using the LS method. Several LS algorithms exist but the simplest and oldest version namely the ordinary least squares (OLS) is sufficient, even if it can perform worse than other alternatives such as the weighted least squares [35]. The goal of OLS is to minimize the error E between the predicted value and true value of the output for the set of data points of size N

$$E = \sum_{i=1}^{N}(Y_i - \hat{Y}_i)^2 = \sum_{i=1}^{N}(Y_i - (kX_i + m))^2 \tag{2.19}$$

which can be achieved by finding the parameters that produce the smallest error. This can be achieved by finding the solution where the derivative is equal to zero i.e. solves the normal equations

$$\frac{\partial E}{\partial m} = 2Nm + 2k\sum_{i=1}^{N} X_i - 2\sum_{i=1}^{N} Y_i = 0 \tag{2.20}$$

$$\frac{\partial E}{\partial k} = 2k\sum_{i=1}^{N} X_i^2 + 2m\sum_{i=1}^{N} X_i - 2\sum_{i=1}^{N} Y_i X_i = 0 \tag{2.21}$$

where from the intersection m and slope k can be derived accordingly

$$m = \bar{Y} - k\bar{X} \tag{2.22}$$

$$k = \frac{\sum_{i=1} N(Y_i - \bar{Y})(X_i - \bar{X})}{\sum_{i=1} N(X_i - \bar{X})^2} \tag{2.23}$$

with the $\bar{X}$ and $\bar{Y}$ represents the average values of the input and output.

2.4 Rough PI-coefficient estimation

According to [36], a successful method of roughly estimating the parameters by using rated data is suggested. With help of the information from the motor nameplate, including rated power P_N, rated current I_N and rated voltage U_N the PI coefficients for the d-axis current regulator can be obtained. The resistance can be obtained by

$$R_s = \frac{P_N}{3{I_N}^2}\frac{1-\eta}{\eta}\gamma. \tag{2.24}$$

The copper loss γ is chosen to a value between 1/2 and 2/3, which has been studied in several studies and motor design manuals, including [37]. η is the efficiency of the motor and varies between 80 and 95 % depending on designer choices [37].

From the voltage equations (2.14) and (2.15) the rough estimation for inductance can be derived. For simplification, $L_m = L_d = L_q$ is assumed only in the parameter identification process. The d-q axis voltage equations' quadratic sum is

$${U_d}^2 + {U_q}^2 = (R_s I_d + X_d I_q)^2 + (E_0 - I_d X_d + I_q R_s)^2 \tag{2.25}$$

where the inductive reactances in the d-q axis are denoted as X_d, X_q. Since $I_d = 0$,$U_d^2 + U_q^2 = U_N^2$ and R_s have been obtained before, the back emf can be estimated as

$$E_0 = \frac{P_N}{3I_N}. \tag{2.26}$$

The full equation for the rough inductance calculation is then expressed

$$U_N^2 = (X_m I_q)^2 + (E_0 + I_q R_s)^2 \tag{2.27}$$

The PI coefficients of the d-axis current regulator can be designed for offline parameter identification based on the rough resistance and inductance measured. Fig. 2.8 shows the d-axis current loop's equivalent diagram.

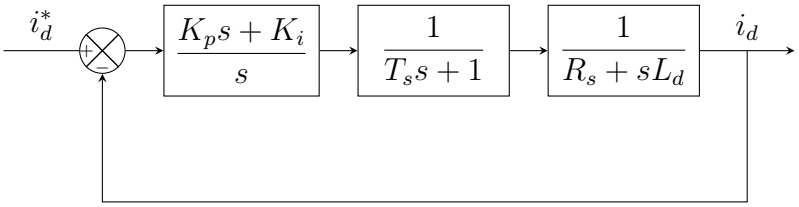

Figure 2.8: Block diagram of the d-axis current loop

The d-axis current loop's PWM period and closed-loop transfer function can be written as

$$G(s) = \frac{i_d}{i_d^*} = \frac{K_p}{T_s L_d s^2 + L_d s + K_p} \tag{2.28}$$

where $K_i = \frac{R_s}{L_d} \cdot K_p$. In this case, the term $T_s L_d s^2$ is so small that the closed-loop transfer function can be considered a first-order system

$$G(s) = \frac{i_d}{i_d^*} = \frac{K_p}{L_d s + K_p} = \frac{K_p / L_d}{s + K_p / L_d} \tag{2.29}$$

According to control theory, the term K_p/L_d is the bandwidth of the current loop. if ω is the bandwidth, K_p can be obtained according

$$\omega_{cb} = K_p / L_d \Rightarrow K_p = \omega_{cb} L_d \tag{2.30}$$

And K_i

$$K_i = \frac{R_s}{L_d} \cdot K_p = \frac{R_s}{L_d} \cdot \omega_{cb} L_d = R_s \omega_{cb} \tag{2.31}$$

3

Case set-up

With the information gathered about the different parameter estimation methods available, and with Aros' wishes and requirements for the estimation, a method was chosen. Since it was desired to not use any extra equipment besides the motor and controller itself for the test and it to be at standstill, a VSI driven SFR method [36] was the most suitable method to use. A lot of the method presented in the upcoming chapter is inspired by [36]. The voltage probing method, presented in Chapter 3.3 is developed as an alternative.

3.1 Roughly estimated PI values

By using equations (2.30) and (2.31), the parameters needed for the PI-regulator are estimated by using rated data of the motor from the datasheet. According to the data sheet for the 12V Demeter motor, the copper loss γ is 1/2 and the motor efficiency is η 90 %. In case the rated data is not available, an alternative method is used, explained further in Chapter 3.3.

Besides the motor used for this project, data from 8 different motors were also used to gather comparison data. These motors have a variety of specifications to gather a wide diversity of motor designs. The specifications of these motors can be seen in Appendix D. When the rough estimations are calculated for the motors, it is necessary to compare the relative error $\hat{E}$ in natural logarithmic scale to make the data more comparable. The relative error is given by

$$|\log(\hat{E})| = |\log(\frac{X_{calc}}{X_N})| \tag{3.1}$$

where X_N is the rated data for each measurement and X_{calc} is the estimated parameter value.

3.2 Parameter identification sequence

The initial rotor position of the PMSM is unknown since no encoder or similar hardware is assumed available, as per the request form Aros . It is possible to determine the rotor position using high-frequency noise as proposed by Holtz [38], however, since the parameter estimation is not required to function on operating motors there is no need for a stationary test which is one of the main advantages of the proposed method. Instead, a current in the d-direction of an arbitrary selected

d-q frame can be applied, and since the motor has no load the rotor will freely align to the applied current resulting in a known rotor position. The current used to align the rotor should be chosen to 80% of I_N, however, if the maximum continuous current for the inverter $I_{N_{MAX}}$ is lower than the I_N this lower value should be used to avoid damage due to over-current. This substitution should be throughout the whole of the method from this point on if such is the case. For our main testing, the d-direction was aligned with the α-phase denoted as 0° however, additional testing was made where the d-direction was rotated 15, 30, and 90 electrical degrees.

With the position of the rotor being known, a locking current of 50 % of the rated current I_N, can be applied in I_d fixating the rotor to the lock position. With the rotor aligned and stationary, the inductance can be determined by measuring the derivative of a current response from an applied signal in the d-direction due to the relationship in (2.14). Since a dynamic current is required, a square noise is superposed onto the locking current, with the amplitude of the noise $U_{_{inj}}$ chosen to a percentage of the rated voltage to avoid over-current increasing from 30% to 70% throughout the two-second measuring time. The square noise is achieved by switching the current direction of the inverter at such a speed that the resulting torque from the currents is negligible and fixating the rotor in the same position. No current regulator is required for the noise since the required voltage is controlled using the duty cycle. The chosen inverter frequency is 8 kHz resulting in a square signal with a frequency ω of 4 kHz. Due to the influence of the inductance, the corresponding current will take the shape of a triangular signal of the same frequency centered around the locking current. By measuring the peak to peak of the triangular signal and dividing it by the corresponding time ΔT, the difference in the linearised derivative can be estimated. By analyzing the dynamic part of (2.14) using the estimated inductance $\hat{L_d}$ and injected noise can be formed

$$U_{d_{inj}} = \hat{L_d}\frac{d(I_d)}{dt} = \hat{L_d}\frac{I_{D_{MAX}} - I_{D_{MIN}}}{\Delta T} \tag{3.2}$$

where the time can be substituted for half of the period which is the inverse of the frequency of the signal ω. Therefore the inductance can be estimated as

$$\hat{L_d} = \frac{2U_{d_{inj}}}{\omega(I_{d_{MAX}} - I_{d_{MIN}})}. \tag{3.3}$$

Following the same approach, the inductance in the q-direction $\hat{L_q}$ can be estimated by rotating the noise 90° electrical to align with the rotors' q-direction leaving the locking-current in the d-direction. With the rotor stationary, the same relationship can be derived from (2.15) as was done in (3.2) resulting in that the inductance for a certain noise amplitude can be estimated from the current-response as

$$\hat{L_q} = \frac{2U_{q_{inj}}}{\omega(I_{q_{MAX}} - I_{q_{MIN}})}. \tag{3.4}$$

Since the frequency ω is constant the inductances L_d, L_q can be calculated by taking the LS of the recorded values from the different noise amplitudes where the input for the algorithm can be chosen as

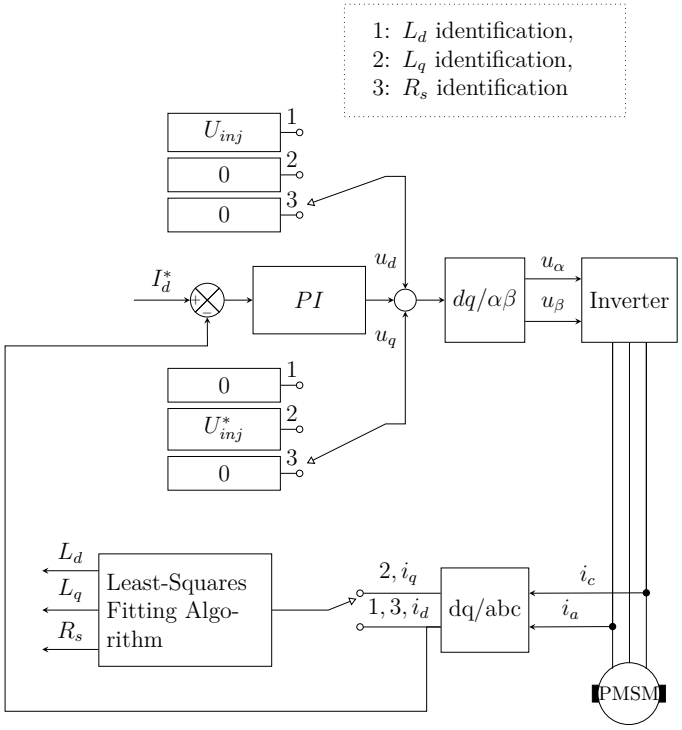

Figure 3.1: Block diagram of the d-axis current loop

$$X_i = \frac{2U_{i_{inj}}}{\omega}, i \in d, q \tag{3.5}$$

while the output is chosen as

$$Y_i = (I_{i_{MAX}} - I_{i_{MIN}}) : i \in d, q \tag{3.6}$$

resulting in the slope k being the inverse of the respective inductances. The algorithm is used to ensure that non-linearities at low or high currents are weighed out and to ensure the reliability of the result.

Estimating the resistance is simpler, due to its possibility to be analyzed at a stationary current as can be derived from (2.14). Therefore the estimated stator resistance $\hat{R}_s$ can be decided by simply measuring the relationship between the applied voltage and the current response

$$U_d = \hat{R}_s I_d \tag{3.7}$$

for the locking current in the d-direction. To filter out the dead-time of the inverter and other non-linearities, measurements are made at incremental locking-currents from 40 % to 140 % of I_N over a two-second period. This allows for the stator inductance R_S similarly to the inductances, to be calculated with the LS algorithm with the input and output were chosen to be the U_d and I_d respectively. This results in that the resistance is the inverse of the slope. An overview of the control circuitry for the three different measurements can be seen in Fig. 3.1 with notably U_{inj}^* being the injected square noise while i_d^* is the desired locking current.

Using the determined parameters it is possible to re-tune the PI regulator in accordance to (2.30), (2.31) and thereafter repeat the procedure. The execution sequence of the parameter identification using a current regulator can be seen in Fig. 3.2.

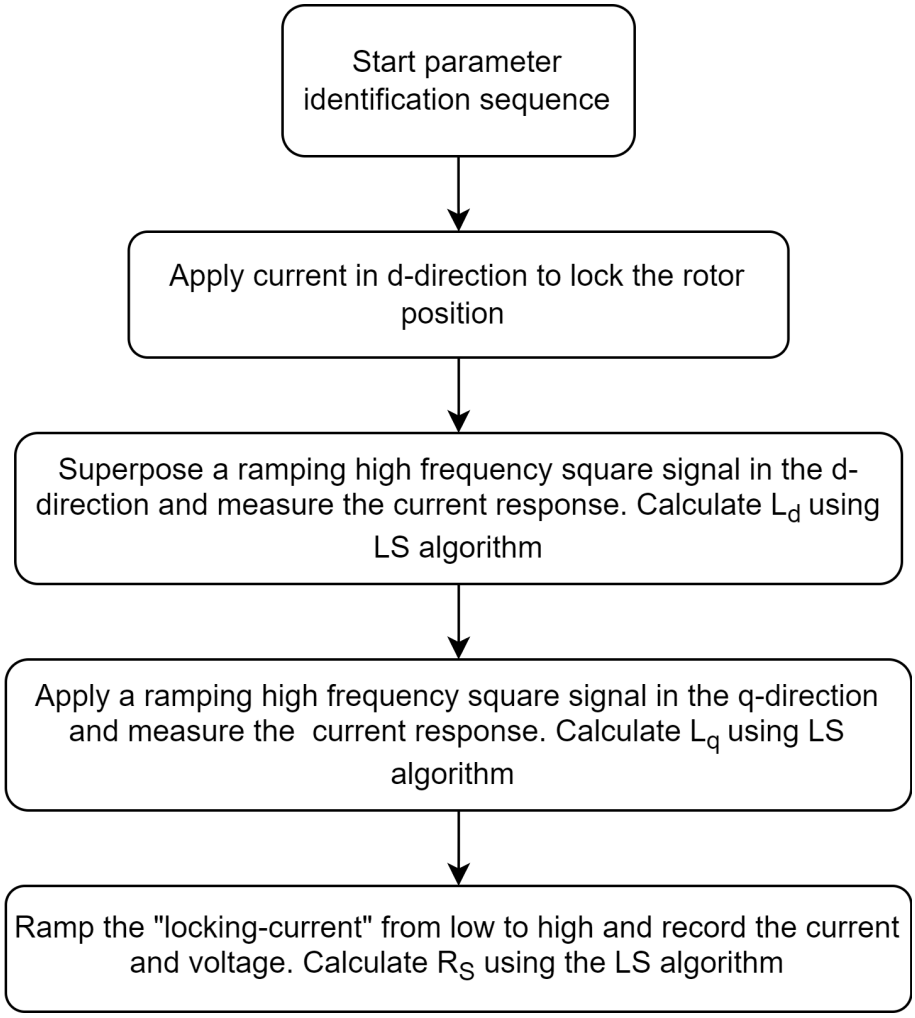

Figure 3.2: Flow chart of the parameter identification sequence

3.3 Voltage probing method

There is a possibility to replace the currently regulated locking current with an alternative method using direct control of the voltages which can be used if insufficient data is available for the rough estimation in Chapter 3.1 or simply as a substitute to it. The method does purely rely on the rated voltage V_N, current I_N, bandwidth ω_{cb} for the motor and maximum current $I_{N_{MAX}}$ for the inverter. Instead of using the current regulator, the voltage is incrementally increased in the d-direction from zero until the current response I_d reaches 50% of I_N or $I_{N_{MAX}}$ depending on the same safety concerns mentioned earlier. Due to the limitation of the software structure, the current and voltage have a resolution of a hundredth of the SI base unit, resulting in an increment of 10 mV being added every 50 milliseconds at a frequency of 20 Hz. Similar to the method mentioned in Chapter 3.2, the rotor will align with

the d-direction due to the induced current and will remain locked by sustaining the corresponding voltage. The alternative locking current is then held for one second to allow both the mechanical and electrical systems to settle and be brought to stationary state, during which the resistance is measured using (3.7). During this measurement, the voltage U_d is kept constant in contrast to the previous resistance measurement. Thereafter the same methodology can be followed for L_d and L_q as described in Chapter 3.2, however, using the alternative locking current instead of the current regulated approach. From the recorded data of the three parameters the temporary parameters $L_{d_{Temp}}$, $L_{q_{Temp}}$ and $R_{S_{Temp}}$ can be calculated using the LS algorithm which subsequently can be applied to (2.30) and (2.31) to create a PI current regulator. An altered overview of the control circuitry for the three different measurements can be seen in Fig. 3.3 with the closed-loop current control being replaced with the direct voltage control to both reach and hold the locking current.

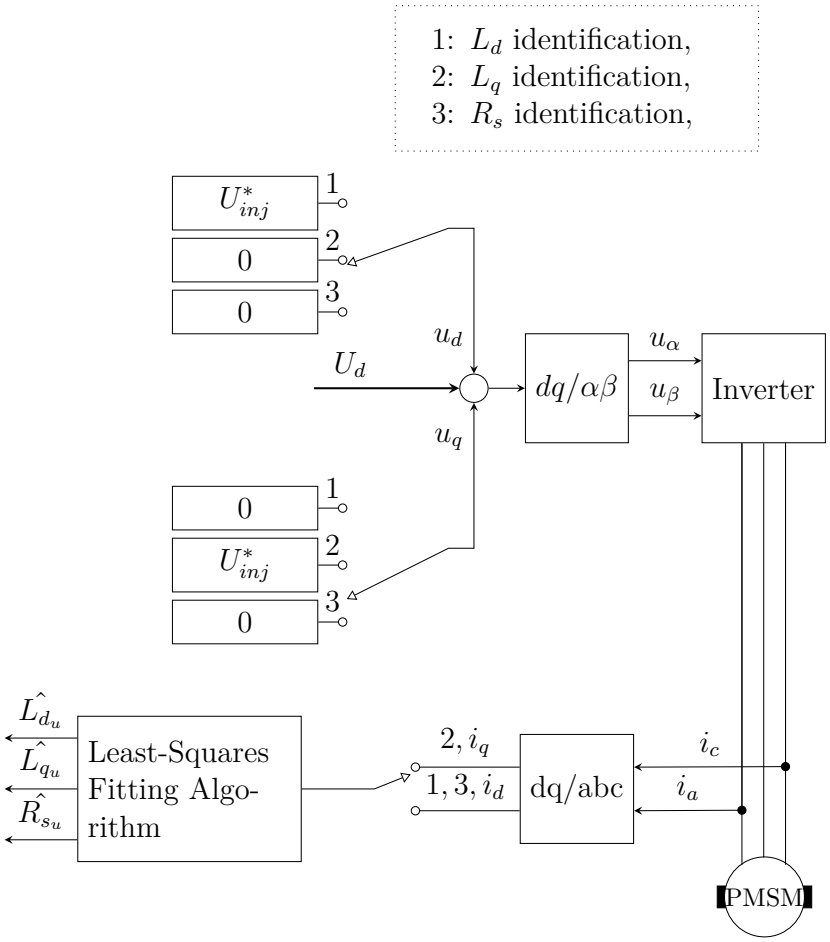

Figure 3.3: Block diagram of the voltage probing method for parameter identification without a current regulator

It is now possible to execute the primary proposed procedure in 3.2 without the need for additional rated data, using the procured current regulator. The summarized methodology proposed in Chapters 3.1, 3.2, and 3.3 is displayed in Fig. 3.4, where the final state references the sequence shown in Fig. 3.2.

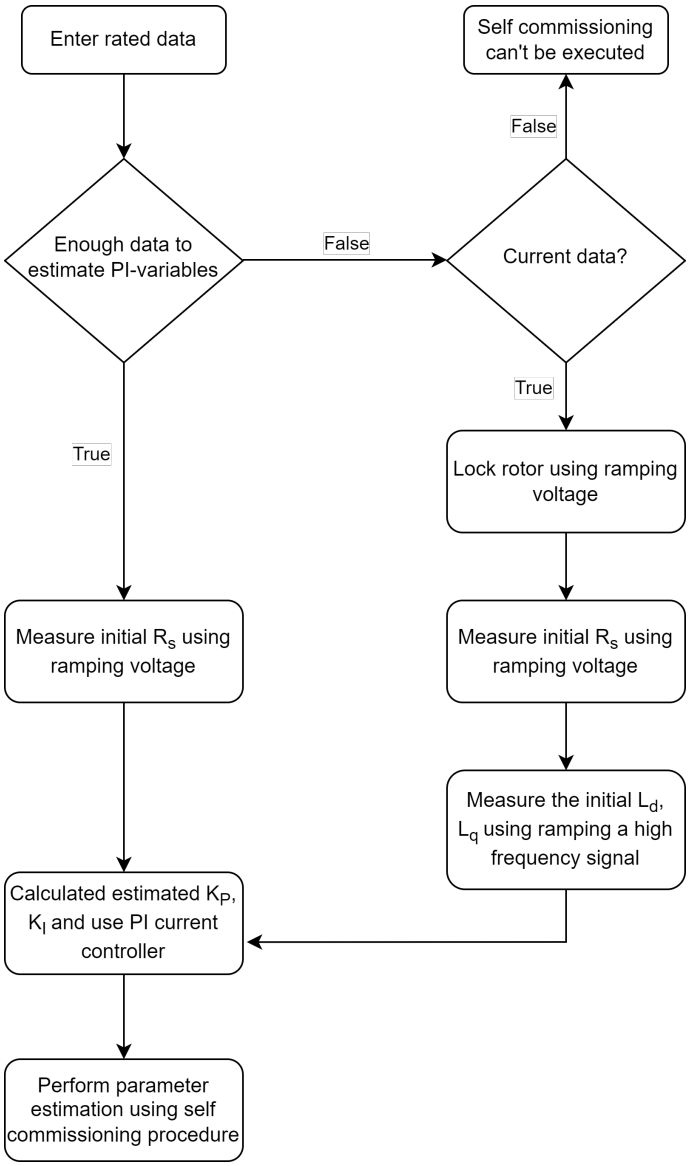

Figure 3.4: Flowchart of the different methods to determine the initial tuning for the current regulator used in the main method

3.4 Simulation setup

Testing the psychical setup is time-consuming and an inaccurate control design might end up damaging the hardware. Therefore, a simulation environment was made to analyze the system in a fast and safe way. This was implemented in Simulink integrated with the control algorithm for the motor.

The motor representation block is made in two different forms. One is a linear model of the motor, taking no nonlinearities into consideration. The other model is derived using the FEM (Finite Element Model) of the 12V motor used during the experiments. It provides a more realistic version of the motor by modeling the nonlinearities. The simulation model can be seen in Appendix C.

3.5 Physical setup

When conduction the physical tests of the algorithm, the a 0.187kW, three-phase, four-pole PMSM with a peak-to-peak voltage of 8.4V is used. Its three phases are connected to Aros proprietary control-board, which houses the microprocessor, with a CPU frequency of 120 MHz and a onboard SRAM with 160 kB of storage. The inverter and it's related electronics are also present on the PCB together with the equipment necessary for communication with operator's computer. The board is powered by a 12V power supply and the current limiter set to 3A to not limit the drawn current from the card, as to allow the maximum current to be decided by the algorithm. An example of the connected hardware is displayed in Fig. 3.5, where the left-most cable is connected to operators computer. The computer is not necessary for the actual execution of the code, however for the algorithm to be run at will with specified input data and to save or display the recorded parameters produced by the algorithm, the computer must be connected. Therefore, the connection is not broken during testing.

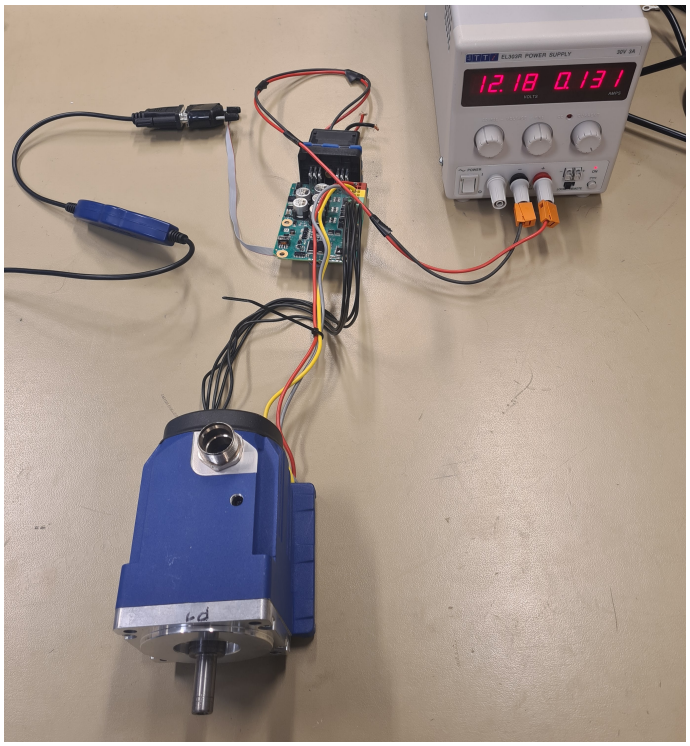

Figure 3.5: Physical setup including power supply, Aros proprietary control board, and the 12V motor

3.6 Aros identification method

As previously discussed, the method currently used for designing or implementing a new PMSM consists of manually measuring the inductance and resistance using exterior measurement equipment. Even though some alternative methods seem to be used by individuals in fringe-cases where exceptionally high accuracy is required,

the primary approach is quite trivial with the inductances and resistances being measured over all three phases using LCR meter, i.e. a combined inductance (L), capacitance (C) and resistance (R) measuring device. For the measurements L_{d_M}, L_{q_M} and R_{S_M} made on the physical motor a LCR-6000 from Good Will Instruments with a accuracy of 0.1%, was used for all three measurements. For the simplest measurement, the determining of the resistance an arbitrarily selected phase is connected to the positive port of the LCR-meter, whereafter the remaining two phases are connected together on the negative port as can be seen in Fig. 3.6 where the initial phase selected as the a-phase.

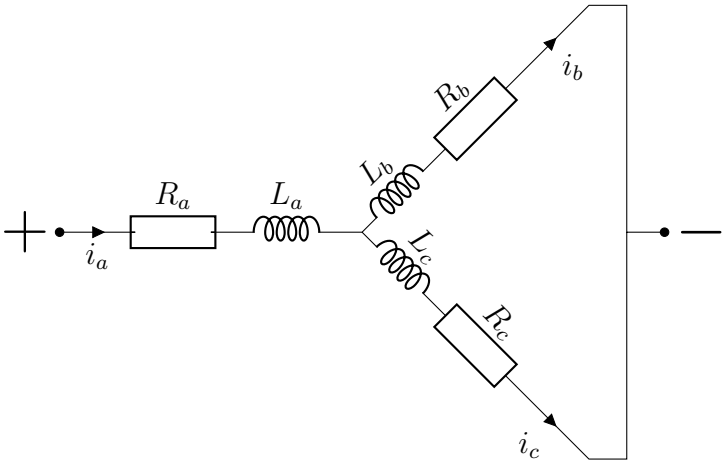

Figure 3.6: How the three phases of the motor are connected to LCR meter

The device then applies 1V over the phases and measures the resulting stationary current with a testing time of a third of a second, i.e. a filtered value is produced at 3 Hz. Thereby the resistance over the three phases R_{abc}, can be calculated according to

$$R_{abc} = \frac{U_{abc}}{I_{abc}} \tag{3.8}$$

where U_{abc} and I_{abc} is the voltage and current over the phases. Since the stator resistances can be assumed ideal the three resistance in the phases are equal, which together with Kirchhoff's law allows the circuitry to be represented by

$$U_{abc} = (R_{S_M} + \frac{1}{\frac{1}{R_{S_M}} + \frac{1}{R_{S_M}}})I_{abc} = \frac{3R_{S_M}}{2}I_{abc}, \tag{3.9}$$

wherefrom, in conjunction with (3.8) the measured stator resistance can be determined to

$$R_{S_M} = \frac{2}{3}R_{abc}. \tag{3.10}$$

For the inductance, the same connection as previously shown in Fig. 3.6 is used but instead of applying a stationary voltage a noise with a frequency 1 kHz is applied over the phases, while the dynamic current response is measured at the

same frequency. The method is similar to the one proposed in Chapter 3.1, however inductance measured is over all three phases resulting in

$$U_{inj_{abc}} = L_{abc}\frac{\Delta I_{abc}}{\Delta T}, \tag{3.11}$$

similar to what is achieved in (3.2). The same conversion with the same reasoning can be made for the inductance as done in (3.9), resulting in the circuitry being expressed by

$$U_{inj_{abc}} = (L_M + \frac{1}{\frac{1}{L_M} + \frac{1}{L_M}})\frac{\Delta I_{abc}}{\Delta T} = \frac{3L_M}{2}\frac{\Delta I_{abc}}{\Delta T} \tag{3.12}$$

resulting in

$$L_M = \frac{2}{3}L_{abc}. \tag{3.13}$$

From this value, the inductance for the d and q-direction is determined by rotating the rotor manually and reading out the values form the LCR meter. The largest value found corresponds to the inductance in the d-direction L_{q_M}, while the smallest is the L_{q_M}. These three values function as a base measurement for a specific motor to compare both to the rated data and the derived parameters from the methods previously proposed.

4

Results

The results will be displayed in the following chapter. The full sequence for the self-commissioning sequence is tested on different setups. The sequence is 13 seconds long and uses the alternative voltage probing estimate instead of calculating the tuning parameters directly from the rated data. The timetable for the described execution is the following:

- 0-2 sec: Ramping up voltage and rough resistance $R_{s_{temp}}$ measuring
- 2-4 sec: High frequency ramping and $L_{d_{temp}}$ measuring
- 4-6 sec: High frequency ramping and $L_{q_{temp}}$ measuring
- 6-6.5 sec: Find rotor sequence
- 6.5-8.5 sec: High frequency ramping and L_d measuring
- 8.5-10.5 sec: High frequency ramping and L_q measuring
- 10.5-12.5 sec: Ramping up current and resistance R_s measuring

The corresponding state-time diagram can be seen in Appendix A, with the calculated parameters including the rated parameters available in Appendix E .

4.1 Simulation result

The results from simulations will be presented in this section. The algorithm executed in the simulation environment using both the linear model and the non-linear FEM model. Figures 4.1, 4.2 show the voltage and current response for the full self-commissioning sequence for the linear model. Figure 4.3 and 4.4 shows the same test but with the non-linear FEM model. The reason why the high-frequency noise is not visible in the software plots 4.3 and 4.1 is because the available current response on the software is taking the average sum of the current value and the previous value.

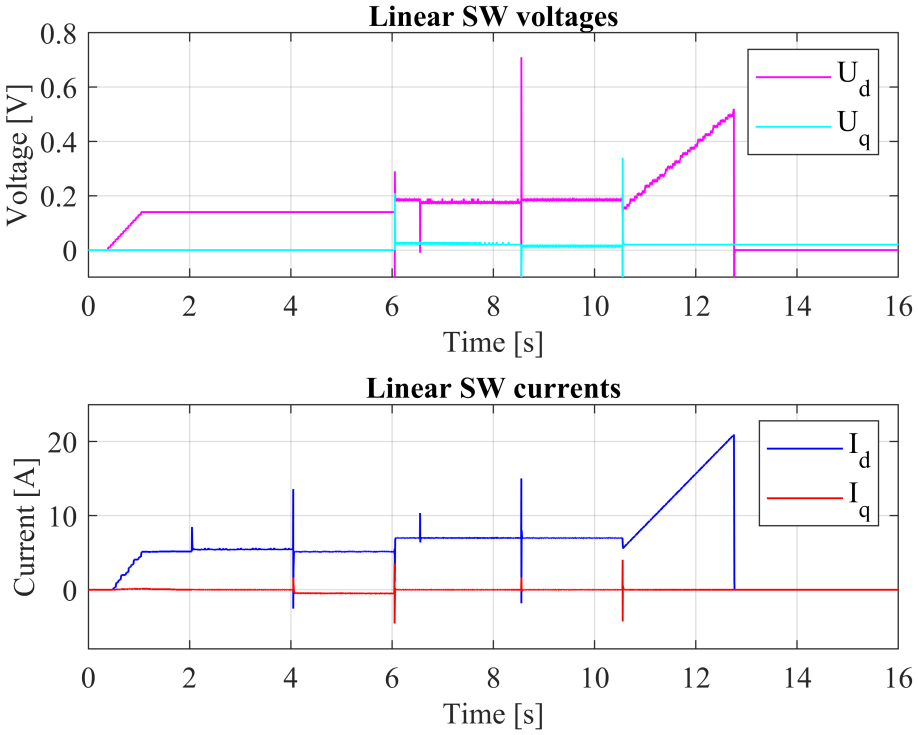

Figure 4.1: Simulation software values from the linear model

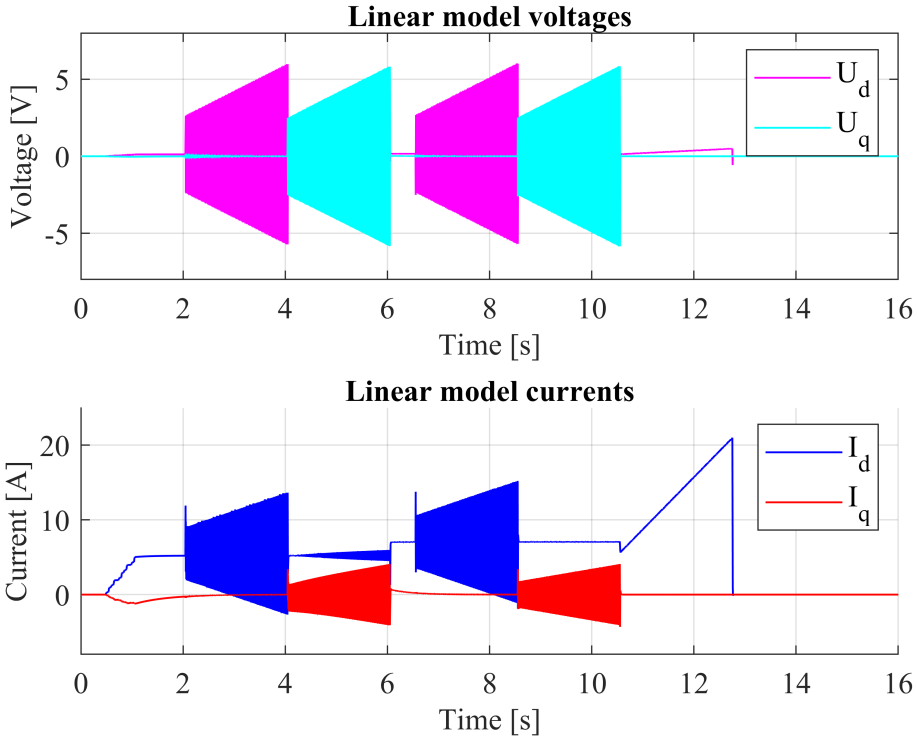

Figure 4.2: Simulation model values from the linear model

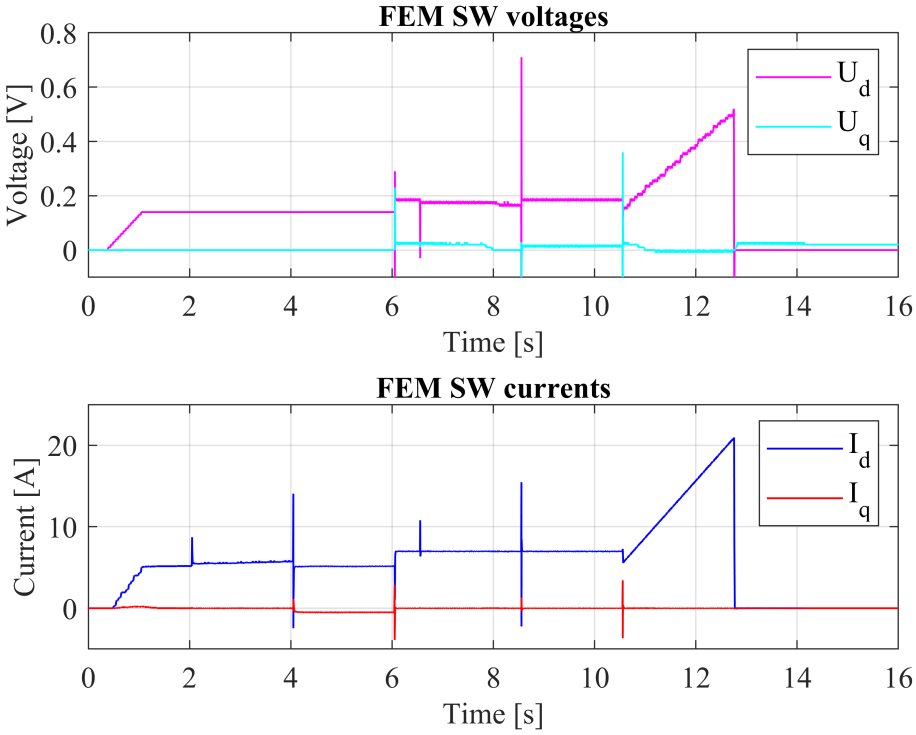

Figure 4.3: Simulation software values from the FEM model

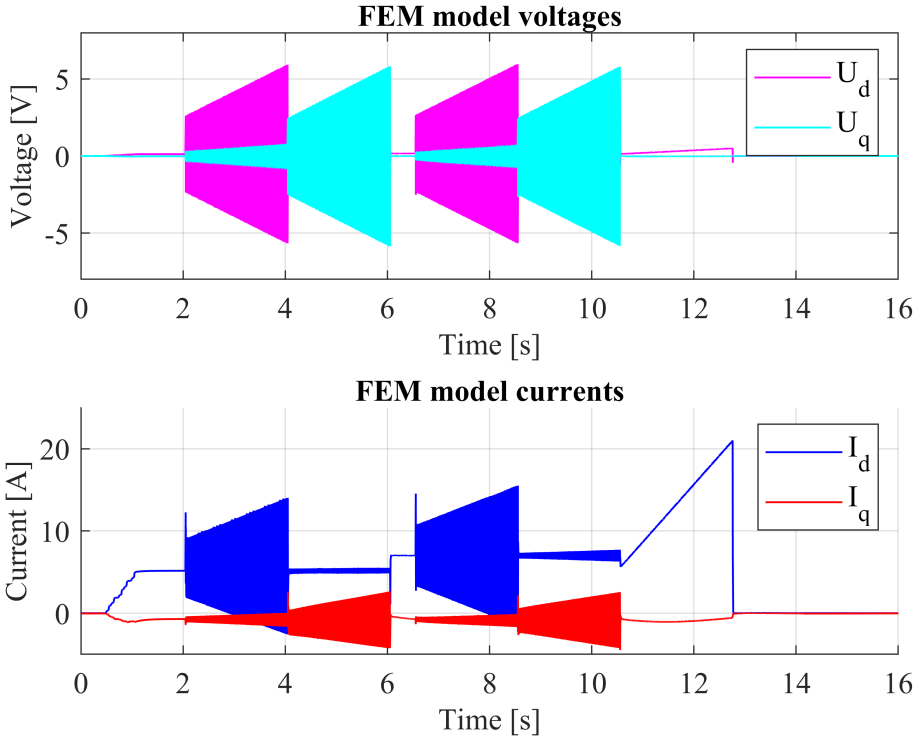

Figure 4.4: Simulation model values from the FEM model

4.2 Physical motor result

The manual measurement method proposed in Chapter 3.6, was executed on the 12V motor and resulted in the inductances $L_{d_M} = 92\mu H$, $L_{q_M} = 183\mu H$ and the resistance $R_{S_M} = 28m\Omega$. These values, together with the rated and the calculated values from the proposed methodology in Chapter 3.2 are displayed in Fig. 4.5 and Fig. 4.6. The rated values are denoted with a N, the measured with a M, the parameters from the voltage probing method's estimation from Chapter 3.3 with the subscript "temp", and finally the calculated values from the parameter identification algorithms in Chapter 3.2, as their base notations. The calculated and voltage probing estimates are derived from the average of the recorded values in Appendix B. Both the calculated and the roughly estimated values were recorded at four different orientations, the proposed orientation where the noise was placed in the d-direction, whereafter it was placed in the q-direction. Three variants of this approach were made, but the locking rotor current was moved 15, 30, and 90 electric degrees respectively, all while the initial orientations of the noises were kept.

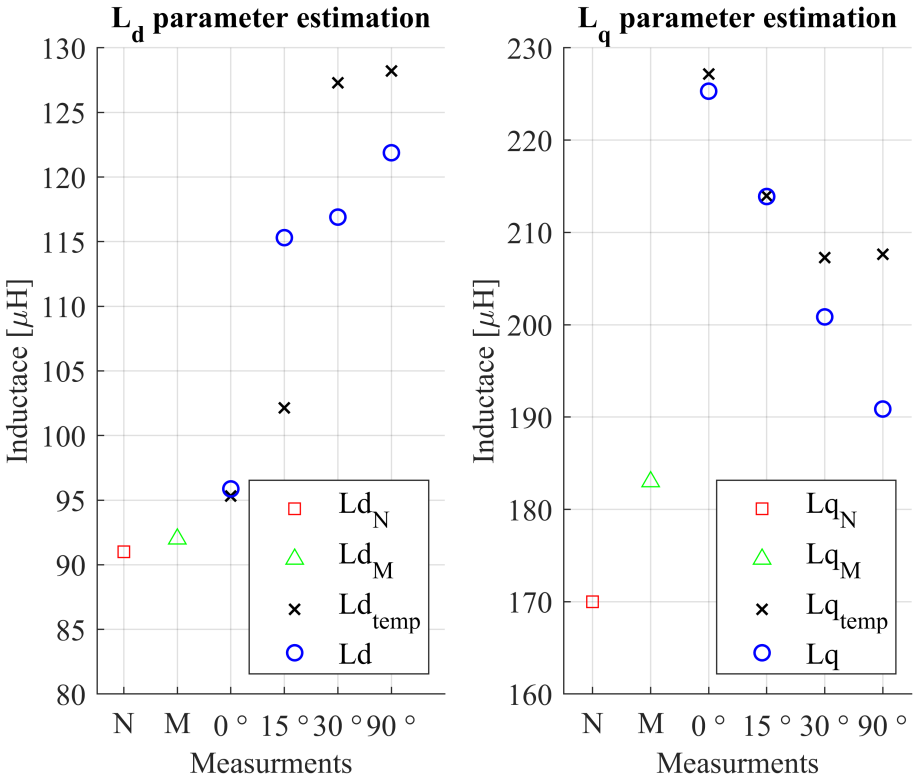

Figure 4.5: Estimated inductances using the algorithm at different locking current positions expressed in electrical degrees compared to the rated and manual measurement

The actual execution of the full sequence, identical to the one used in the simulations, being run on the physical motor can be seen in Fig. 4.7. The average values of the voltages and the currents are recorded every 10ms at a frequency of 100Hz at a resolution of 0.01V and 0.01A respectively.

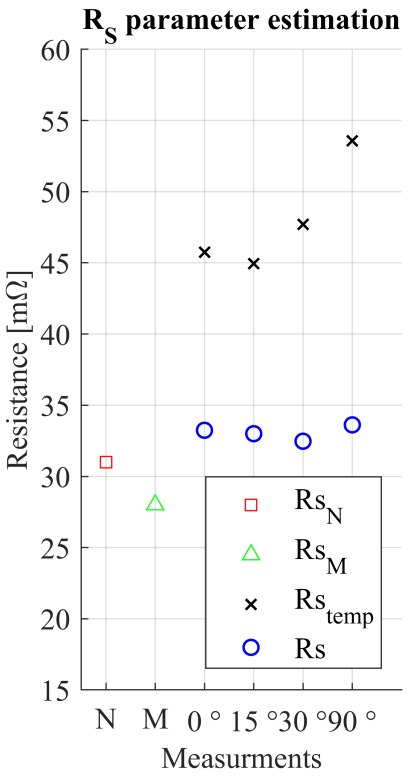

Figure 4.6: Estimated resistance using the proposed algorithm at different locking current positions expressed in electrical degrees compared to the rated and manual measurement

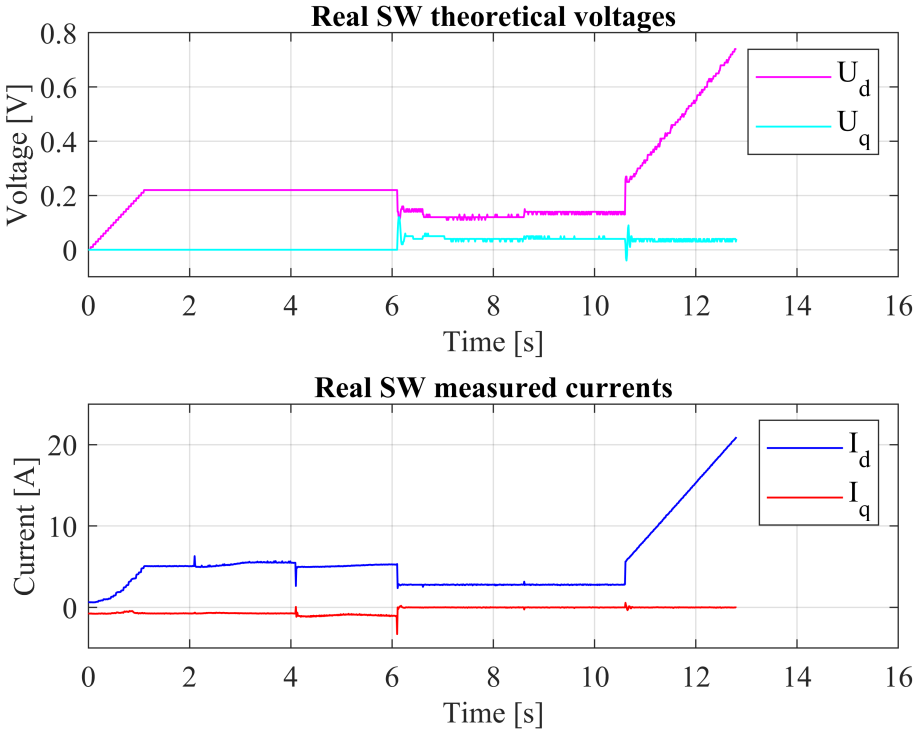

Figure 4.7: Software values from a real test recorded at 100Hz

4.3 Rough parameter estimation

The rough estimation calculations were tried on the motors in Appendix D, which have different characteristics to get a wide result. In the figures 4.8, 4.9 and 4.10 the results are shown for all 9 different motors tested for R_s, L_d and L_q. The values are plotted on an absolute value logarithmic scale of the relationship between the rough estimate and the rated values. This is done to make it possible to compare both errors that are larger and smaller. If the plotted value is 0 there is no difference between the value taken from the motors data sheet and the estimate, i.e. the fraction is equal to one.

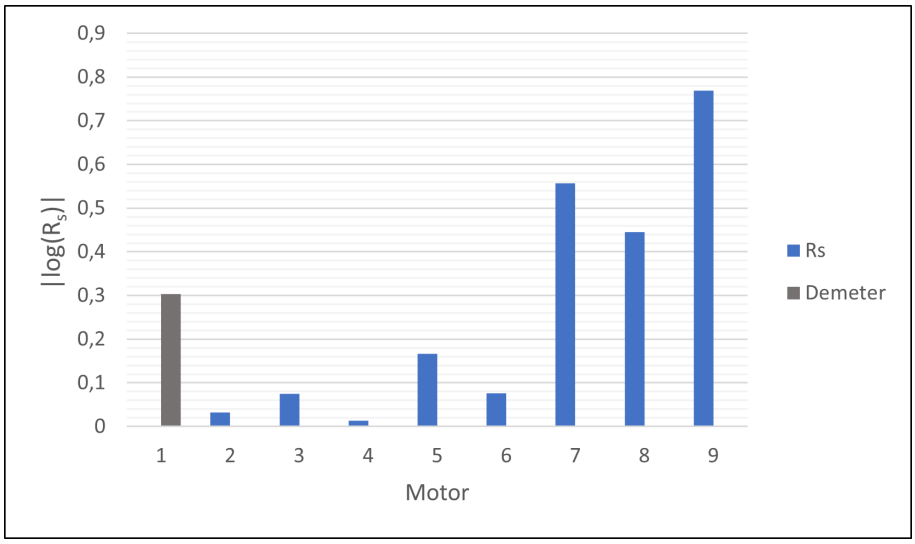

Figure 4.8: Result from rough parameter estimation for the resistance R_s from different motors

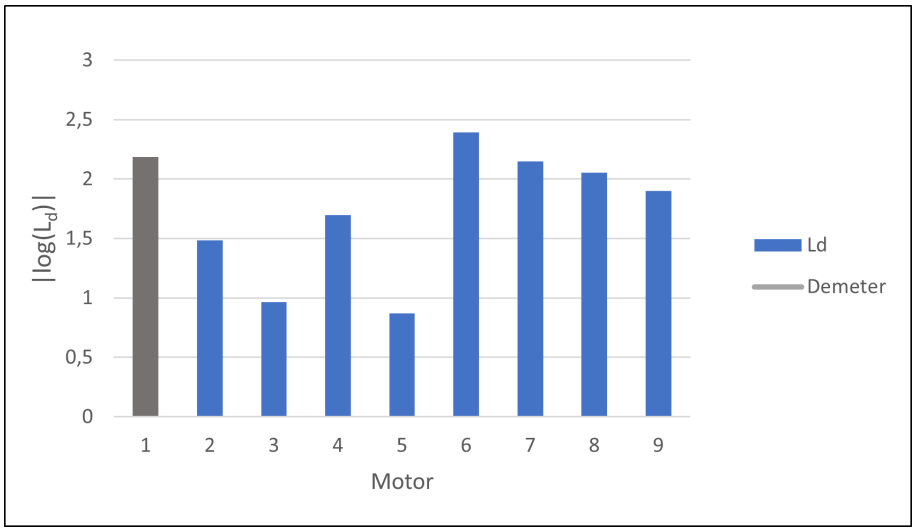

Figure 4.9: Result from rough parameter estimation for the resistance L_d from different motors

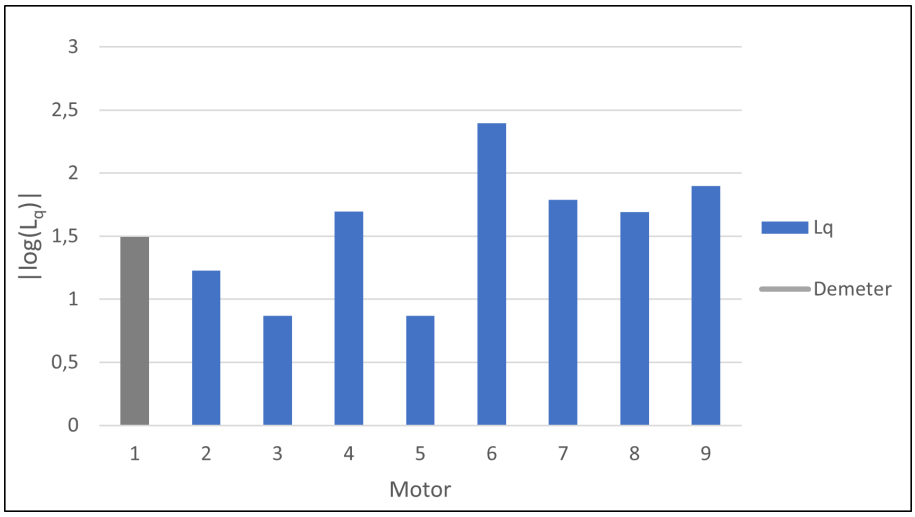

Figure 4.10: Result from rough parameter estimation for the resistance L_q from different motors

5
Discussion

In this chapter, the results presented in Chapter 4 will be discussed in addition to the design choices naturally taken along the methodology's development.

By analyzing the different calculated inductances in Fig. 4.5, a variation is present depending on how the rotor is oriented in relation to the A-phase which is represented by the electrical offset of 0°. The best value for L_d was achieved by having the noise and locking-current both on top of the A-phase, but resulted in the worst L_q. Meanwhile, the best L_q value was found by rotating the rotor 90° such that the q-direction and therefore the applied noise, is placed where the d-direction previously was placed for achieving its best result. This is possibly related to how the actual inductance is measured. As mentioned in the manual measuring method in Chapter 3.6, the inductance is measured from one phase to two, i.e. the noise is applied in one phase. This is essentially what is achieved in the two favorable measurements, where the L_d at 0° is aligned with the A-phase and the L_q at 90° achieves the same orientation in the $\alpha\beta$-coordinate system. This corresponds to the same electrical circuitry that is used for the manual measuring method. This improvement in L_q and deterioration of L_d is visible throughout the measurements in Fig. 4.5, indicating that there is a proportional relationship between the angle and errors compared to the measured values. As previously discussed a dead-time is present for the inverter which lowers the produced voltage since no current flows when at least one of the two switches is open. This can lead to issues when applying low voltages since the produced error can become a non-negligible part of the signal, it is therefore important to apply a sufficiently high voltage when measuring the resistance. If the theoretical applied voltage diverges significantly from the true, the measured current will produce a result indicating a larger resistance than is in fact present. This is the main reason for the arguably high current levels for the resistance measurements and varying the levels during the tests, to filter out similar issues. This could be one of the explaining factors for the higher resistance in Fig. 4.6 since the dead-time would have produced a lower current that would result in a larger resistance according to (3.7).

As mentioned in 4.2 the recorded values are the average of the currents and voltages and therefore don't accurately represent either the voltages or the currents. It would theoretically be possible to record better-representing values by increasing the recording frequency but this would require significantly more memory over the 13-second short recording. If every peak for the currents and voltages would be recorded at a frequency of 8kHz, over 6MB would be required, more the 40 times the onboard memory. This higher recording frequency would not improve the actual

algorithm and only provide marginally more descriptive data. Therefore the choice was made to not implement this possible feature.

When comparing the rough estimates for R_S, L_d and L_q in Figures 4.9, 4.10, 4.8 respectively, the logarithmic scale was chosen over for example a percentage-based scale. This is since when comparing larger and smaller values than the base value, the error in percentages is not comparable when analyzing potentially large differences. If the comparing value is off by a factor of two it can be represented as the natural logarithm $\approx \pm 0.693$, importantly the absolute value is the same in either direction. While for the percentages, it would be an increase of 100% or a decrease of 50%. The method used for these estimates, proposed by Wang et. al. [36] seems to not reliably produce usable parameters for tuning, based on the fairly limited but diverse selection of motors. The R_S estimate produced in the paper is near perfect as can be seen for motors 2 and 4 in Fig. 4.8, while the largest error produced by our testing, motor 9 had an error of approximately a factor of two compared to its rated values. A non-negligible error but would allow for the initial tuning of the PI-regulator. The estimated inductances on the other hand proved to be unreliable since a majority of the motors produced too large of an error in both directions. Since the proportional parameter for the controller depends on L_d as can be seen in (2.30), it is most interesting to focus on only this parameter. Through simulations, it was discovered that the system became uncontrollable with a L_d error corresponding with a value of 1.5 on the logarithmic scale, i.e. approximately a divergence of a factor 4.5. The fact that the corresponding cutoff value for the R_S parameters is much larger together with its recorded low average error from Chapter 4, the conclusion is drawn that the L_d value is the determining parameter. Wang et. al. arrived at an estimate of L_d that was a factor of approximately 4.3 larger than the rated value, just within the logarithmic cutoff value of 1.5. Six of the tested motors failed this limit, as can be seen in Fig. 5.1 where the red dotted line is the previously mentioned cutoff value for the system to be controllable. The motors that failed with the proposed method, including the 12V motor, generated too large of an error. The mentioned cutoff level was chosen based on parameter manipulation done when simulating the 12V motor, so it is possible that a larger motor such as the 380V used by Wang et. al. would have electrical and mechanical properties that could handle such large discrepancies but this cannot be shown in the work done in this paper or is presented in the paper by Wang et. al. [36]. Due to the poor estimations, the alternative method for rough estimation using a voltage probing approach was explored and tested to produce a working self-commissioning sequence.

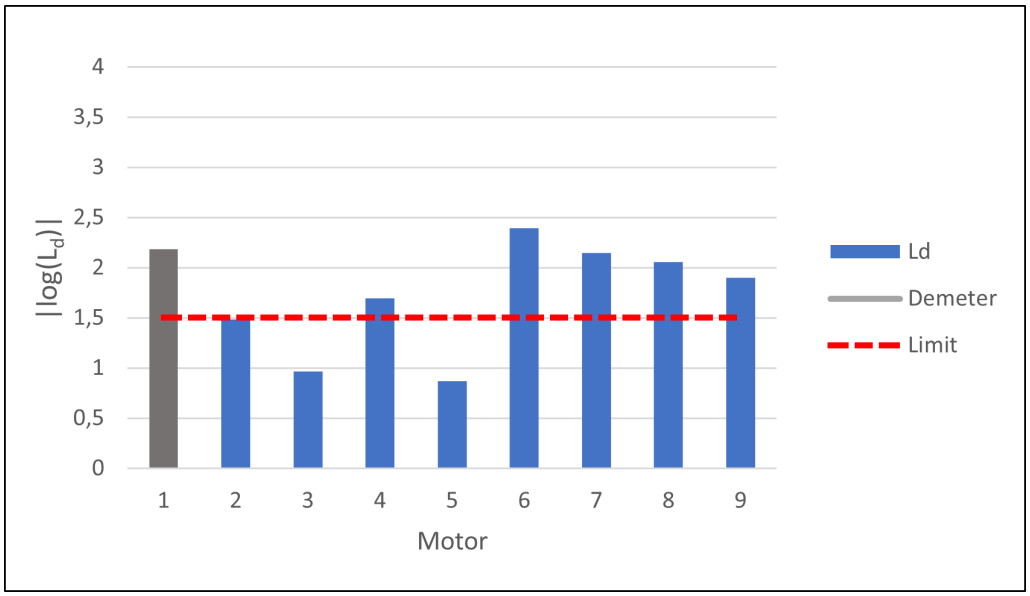

Figure 5.1: Result from rough parameter estimation for the resistance L_d from different motors, with the limit found for a well behaving PI regulator

This method could also be used as a fault diagnostics tool to check the condition of the motor's hardware. By detecting damaged wiring or magnets caused by mechanical deterioration in an early state of the damage, the motor can be repaired instead of replaced contributes to more sustainable thinking. By limiting wear and tear and potential failures a better planned maintenance could be designed to limit shipping and travel.

Another area of usage for the self-commissioning sequence is to measure the stator resistance and stator inductances for motors with inadequate information about the motor since our method requires only rated data. This will make it available to use motors for more complex cases whereas a controller is needed and would not be possible to use in other cases. We believe that the work conducted in this thesis does create any ethical quandaries and that the data and sources are presented in a truthful and honest manor.

6
Conclusion and future work

6.1 Conclusion

In this thesis, a self commissioning sequence method is tested and verified. The electrical stator parameters R_s, L_d and L_q are estimated on a PMSM motor.

It is shown that the inductances L_d and L_q together with the stator resistance R_S can be estimated accurately enough to tune a well-behaving PI current regulator. However, the results from calculations in Chapter 4 show that the rough parameter estimation does not work for the 12V test motor. The comparison study done shows that it would work on certain motors with different specifications but a majority of the examined PMSMs failed, ruling out the method as reliable. Instead, an alternative voltage probing method can be applied to initially estimate the parameters necessary for a PI regulator, which is utilized in the main current-controlled test which produces a lower parameter error.

Finally, it can be shown that rotating the rotor to align the theoretical inductance positions with a phase of the motor, increases the accuracy of the inductance. Therefore, the highest accuracy is achieved by completing the full method proposed using the initial voltage probing whereafter the locking current is manipulated such that both noises align with a single phase.

6.2 Future work

Much more may be examined, as is often the case. The following section outline some potential future research for the thesis.

- There could be a possible improvement to the current measurements if sweeping measurements were conducted, where instead of only recording the measurement at the theoretical rotor position using the locking current, additional measurements are made within the proximity of the point of interest. This could for example find a lower inductance when searching for the L_d, which would indicate that the rotor is not perfectly aligned with the applied noise.
- We have only considered the calculations for resistance and inductance. In a motor parameter identification process, the next step would be to estimate the inertia J and the magnet flux linkage Ψ_m and can be built upon our work to extend the method

- The method was only tested on one 12 V motor. An comparison study with tests on a variety of motors would be interesting and could conclude in more concrete information about the method's robustness.

Bibliography

[1] L. G. X. J. X. L. Z. Wang, B. Yao and H. Wang, "Initial rotor position detection for permanentmagnet synchronousmotor based on high-frequency voltage injection without filter," *World Electric Vechicle Journal*, 2020.

[2] M. A. A. C. O. Saadaouia, A. Khlaiefa and M. Boussakb, "A sliding-mode observer for high-performance sensorless control of pmsm with initial rotor position detection," *International journal of control*, vol. 90, no. 2, 2020.

[3] N. Imai, S. Morimoto, M. Sanada, and Y. Takeda, "Influence of magnetic saturation on sensorless control for interior permanent-magnet synchronous motors with concentrated windings," *IEEE Transactions on Industry Applications*, vol. 42, no. 5, pp. 1193–1200, 2006.

[4] M. A. Khan, I. Husain, R. Islam, and J. Klass, "Design of experiments to address manufacturing tolerances and process variation influencing cogging torque and back emf in the mass production of the permanent magnet synchronous motors," in *2012 IEEE Energy Conversion Congress and Exposition (ECCE)*, 2012, pp. 3032–3039.

[5] D. Fernandez, D. Hyun, Y. Park, D. Reigosa, S. B. Lee, D. M. Lee, and F. Briz, "Permanent magnet temperature estimation in pm synchronous motors using low cost hall effect sensors," in *2016 IEEE Energy Conversion Congress and Exposition (ECCE)*, 2016, pp. 1–8.

[6] D. Fernández, M. Martínez, D. Reigosa, J. M. Guerrero, C. M. Suárez Alvarez, and F. Briz, "Impact of machine magnetization state on permanent magnet losses in permanent magnet synchronous machines," *IEEE Transactions on Industry Applications*, vol. 55, no. 1, pp. 344–353, 2019.

[7] J. Wang, W. Wang, K. Atallah, and D. Howe, "Demagnetization assessment for three-phase tubular brushless permanent-magnet machines," *IEEE Transactions on Magnetics*, vol. 44, no. 9, pp. 2195–2203, 2008.

[8] Y. Xu, N. Parspour, and U. Vollmer, "Torque ripple minimization using online estimation of the stator resistances with consideration of magnetic saturation," *IEEE Transactions on Industrial Electronics*, vol. 61, no. 9, pp. 5105–5114, 2014.

[9] M. S. Rafaq and J.-W. Jung, "A comprehensive review of state-of-the-art parameter estimation techniques for permanent magnet synchronous motors in wide speed range," *IEEE Transactions on Industrial Informatics*, vol. 16, no. 7, pp. 4747–4758, 2020.

[10] "Ieee standard procedures for obtaining synchronous machine parameters by standstill frequency response testing," *IEEE Std 115A-1987*, pp. 1–28, 1987.

[11] E. Eitelberg and R. G. Harley, "Estimating synchronous machine electrical parameters from frequency response tests," *IEEE Transactions on Energy Conversion*, vol. EC-2, no. 1, pp. 132–138, 1987.

[12] A. Keyhani, S. Hao, and R. Schulz, "Maximum likelihood estimation of generator stability constants using sser test data," *IEEE Transactions on Energy Conversion*, vol. 6, no. 1, pp. 140–154, 1991.

[13] O. Wallscheid and J. Böcker, "Global identification of a low-order lumped-parameter thermal network for permanent magnet synchronous motors," *IEEE Transactions on Energy Conversion*, vol. 31, no. 1, pp. 354–365, 2016.

[14] K. Miyashita, S. Yamashita, S. Tanabe, T. Shimozu, and H. Sento, "Development of a high speed 2-pole permanent magnet synchronous motor," *IEEE Transactions on Power Apparatus and Systems*, vol. PAS-99, no. 6, pp. 2175–2183, 1980.

[15] V. Honsinger, "The fields and parameters of interior type ac permanent magnet machines," *IEEE Transactions on Power Apparatus and Systems*, vol. PAS-101, no. 4, pp. 867–876, 1982.

[16] J. Gieras, *PERMANENT MAGNET MOTOR TECHNOLOGY: DESIGN AND APPLICATIONS*, 01 2010.

[17] R. Dutta and M. Rahman, "A comparative analysis of two test methods of measuring*d*- and*q*-axes inductances of interior permanent-magnet machine," *IEEE Transactions on Magnetics*, vol. 42, no. 11, pp. 3712–3718, 2006.

[18] P. Mellor, F. Chaaban, and K. Binns, "Estimation of parameters and performance of rare-earth permanent-magnet motors avoiding measurement of load angle," *Electric Power Applications, IEE Proceedings B*, vol. 138, pp. 322 – 330, 12 1991.

[19] S. A. Odhano, R. Bojoi, E. Armando, G. Homrich, A. F. F. Filho, M. Popescu, and D. G. Dorrell, "Identification of three-phase ipm machine parameters using torque tests," *IEEE Transactions on Industry Applications*, vol. 53, no. 3, pp. 1883–1891, 2017.

[20] ——, "Identification of three-phase ipm machine parameters using torque tests," *IEEE Transactions on Industry Applications*, vol. 53, no. 3, pp. 1883–1891, 2017.

[21] S. A. Odhano, R. Bojoi, G. Roşu, and A. Tenconi, "Identification of the magnetic model of permanent-magnet synchronous machines using dc-biased low-frequency ac signal injection," *IEEE Transactions on Industry Applications*, vol. 51, no. 4, pp. 3208–3215, 2015.

[22] P. Zhou, M. Rahman, and M. Jabbar, "Field circuit analysis of permanent magnet synchronous motors," *IEEE Transactions on Magnetics*, vol. 30, no. 4, pp. 1350–1359, 1994.

[23] K. J. Meessen, P. Thelin, J. Soulard, and E. A. Lomonova, "Inductance calculations of permanent-magnet synchronous machines including flux change and self- and cross-saturations," *IEEE Transactions on Magnetics*, vol. 44, no. 10, pp. 2324–2331, 2008.

[24] J.-Y. Lee, S.-H. Lee, G.-H. Lee, J.-P. Hong, and J. Hur, "Determination of parameters considering magnetic nonlinearity in an interior permanent magnet

synchronous motor," *IEEE Transactions on Magnetics*, vol. 42, no. 4, pp. 1303–1306, 2006.

[25] G.-H. Kang, J.-P. Hong, G.-T. Kim, and J.-W. Park, "Improved parameter modeling of interior permanent magnet synchronous motor based on finite element analysis," *IEEE Transactions on Magnetics*, vol. 36, no. 4, pp. 1867–1870, 2000.

[26] M. Elbuluk, T. Liu, and I. Husain, "Neural network-based model reference adaptive systems for high performance motor drives and motion controls," in *Conference Record of the 2000 IEEE Industry Applications Conference. Thirty-Fifth IAS Annual Meeting and World Conference on Industrial Applications of Electrical Energy (Cat. No.00CH37129)*, vol. 2, 2000, pp. 959–965 vol.2.

[27] W. Shaowei and W. Shanming, "Identify pmsm's parameters by single-layer neural networks with gradient descent," in *2010 International Conference on Electrical and Control Engineering*, 2010, pp. 3811–3814.

[28] L. Liu, D. A. Cartes, and W. Liu, "Particle swarm optimization based parameter identification applied to pmsm," in *2007 American Control Conference*, 2007, pp. 2955–2960.

[29] M.-w. Qian, G.-j. Tan, and Z. Ling, "Parameter identification of pmsm based on fhpso algorithm," in *2010 2nd International Conference on Information Engineering and Computer Science*, 2010, pp. 1–4.

[30] H. Toliyat, E. Levi, and M. Raina, "A review of rfo induction motor parameter estimation techniques," *IEEE Transactions on Energy Conversion*, vol. 18, no. 2, pp. 271–283, 2003.

[31] L. Harnefors, "Control of power electronic converters and variable-speed drives," Västerås, Sweden, Department of Electronics, Mälardalens University, 2002.

[32] E. Gurpinar and A. Caste, "Single-phase t-type inverter performance benchmark using si igbts, sic mosfets, and gan hemts," *IEEE TRANSACTIONS ON POWER ELECTRONICS*, vol. 1, no. 10, 2016.

[33] Björck, "Algorithms for linear least squares problems," *Computer Algorithms for Solving Linear Algebraic Equations*, pp. 57–92, 1990.

[34] F. L. Severence, *System modeling and simulation: An introduction*, 1st ed. Chichester, West Sussex, England: John Wiley & Sons Ltd, 2001.

[35] H. Abdi, "The method of least squares," *Encyclopedia of measurement and statistics*, vol. 1, pp. 530–532, 2007.

[36] G. Wang, L. Qu, H. Zhan, J. Xu, L. Ding, G. Zhang, and D. Xu, "Self-commissioning of permanent magnet synchronous machine drives at standstill considering inverter nonlinearities," *IEEE Transactions on Power Electronics*, vol. 29, no. 12, pp. 6615–6627, 2014.

[37] A. T. De Almeida, F. J. T. E. Ferreira, and J. A. Fong, "Standards for efficiency of electric motors," *IEEE Industry Applications Magazine*, vol. 17, no. 1, pp. 12–19, 2011.

[38] J. Holtz, "Acquisition of position error and magnet polarity for sensorless control of pm synchronous machines," *IEEE Transactions on Industry Applications*, vol. 44, no. 4, pp. 1172–1180, 2008.

A

State-time diagram

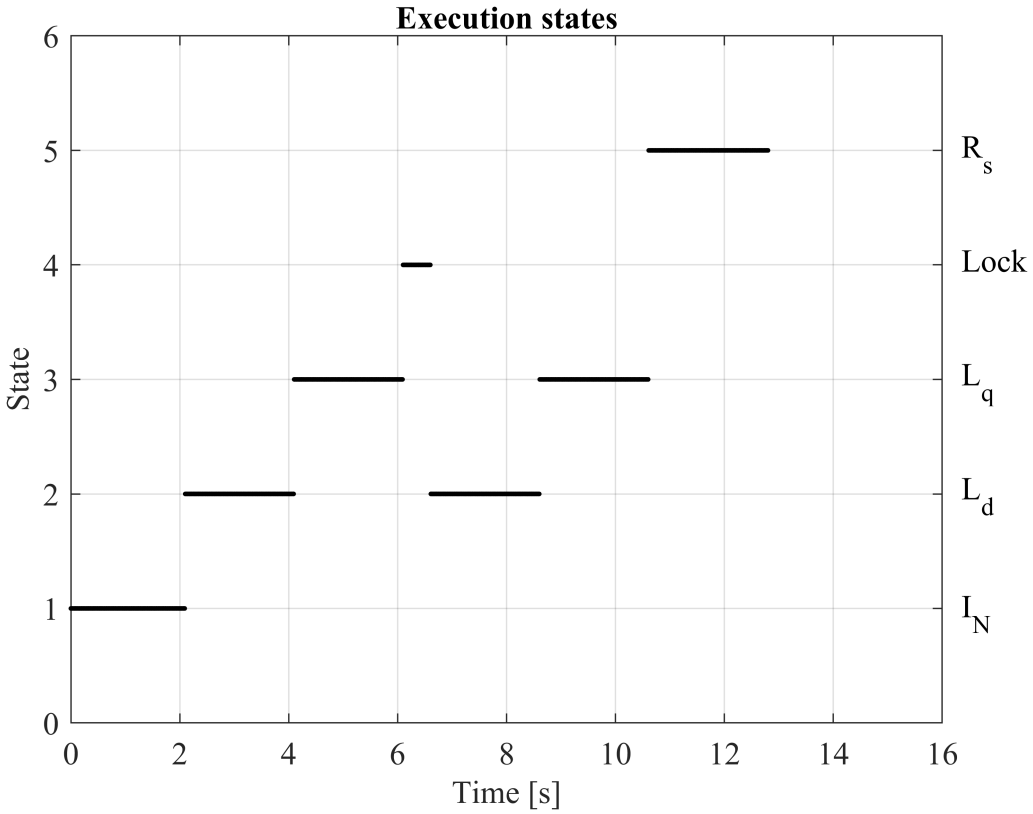

Figure A.1: How the self-commissioning algorithm executes the different sequences as described for the tests

B

Physical motor results

Test	1	2	3	4	5	Unit
$L_{d_{Temp}}$	94.57	92.58	94.85	92.82	94.83	μH
L_d	122.54	122.20	122.58	123.66	123.14	μH
$L_{q_{Temp}}$	226.49	226.97	227.16	227.09	227.02	μH
L_q	204.51	203.78	201.78	201.20	202.83	μH
R_{Temp}	43.05	43.14	43.05	43.05	43.48	mΩ
R	32.80	32.82	32.85	32.87	32.89	mΩ

Table B.1: Recorded values from physical tests on the 12V motor using the proposed current controlled method, with no rotor offset for either the L_d or L_q measurments

C
Simulation model

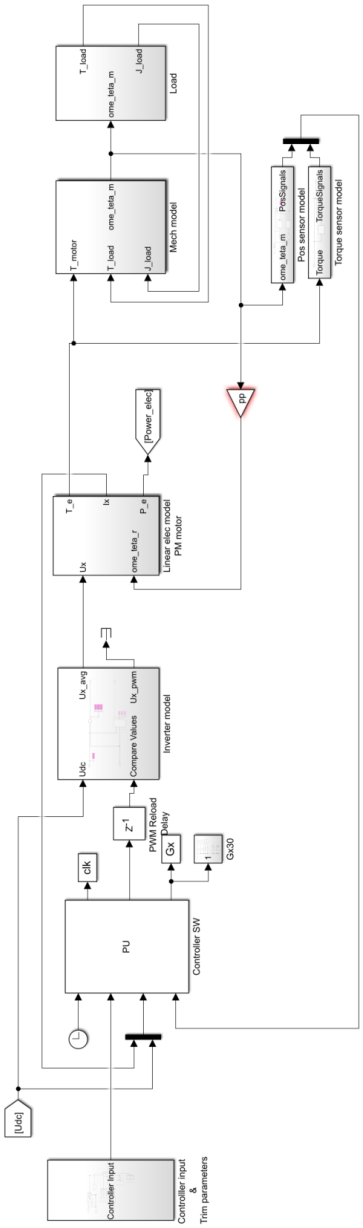

Figure C.1: Simulink

D

Motor data

Motor	$Speed_R$	V_R	I_R	P_R	$NrPoles$	$L_{d_{rated}}$	$L_{q_{rated}}$	R_R	η
Demeter	3000	8,4	13,975	0,183	4	0,09	0,18	0,0235	90
Paper-Motor	1000	380	37,2	22	22	1,7	2,2	0,135	95
DS2-100BO54W-25-5	2500	365	76	41	6	2	2,2	0,096	93
DSD2-045SO64U-30-54	3000	335	1,56	0,73	8	27	27	9,4	84
DSD2-071BO64W-20-54	2000	320	44,4	16	8	3,3	3,3	0,26	86
DSD 045 S 64 U 30-5	3000	540	1,4	0,63	8	26,7	26,7	10,2	85
SUS1	3000	7,66	39,44	0,471	4	0,03	0,043	0,012	88
SUS2	4000	17,8	75,68	2,1	4	0,03	0,043	0,013	88
BTG-Mek-3000	800	17,8	6,01	0,167	8	1,1	1,1	0,226	88

Table D.1: Specifications for the different motors tested

E

Parameter results

	Rough est.	Linear	Non-linear	Psychical	Alt. rough est. (1)	Rated	Measured	
L_d	799	89	85	96	95	91	92	μF
L_q	799	176	20	225	227	170	183	μF
R_s	17,5	27	23	33	46	31	28	$m\Omega$

Table E.1: Results for all the different tests performed

DEPARTMENT OF SOME SUBJECT OR TECHNOLOGY
CHALMERS UNIVERSITY OF TECHNOLOGY
Gothenburg, Sweden
www.chalmers.se

CHALMERS
UNIVERSITY OF TECHNOLOGY